

Final Report

**IMPLEMENTATION OF AN ALTERNATIVE
PLUME RISE METHODOLOGY IN CAMx**

Work Order No. 582-7-84005-FY10-20

Prepared for

Texas Commission on Environmental Quality
12118 Park 35 Circle
Austin, Texas 78753

Prepared by

Christopher Emery
Jaegun Jung
Greg Yarwood

ENVIRON International Corporation
773 San Marin Drive, Suite 2115
Novato, CA 94998

June 11 2010

TABLE OF CONTENTS

	Page
EXECUTIVE SUMMARY	ES-1
1. INTRODUCTION.....	1-1
1.1 Background.....	1-1
1.2 Overview of Plume Rise Calculations	1-2
2. SUMMARY OF PLUME RISE ALGORITHMS.....	2-1
2.1 CAMx	2-1
2.2 SMOKE/CMAQ	2-2
2.3 CALPUFF	2-3
2.4 AERMOD	2-3
2.5 Original Recommendation for CAMx	2-4
3. 3. COMPARISON OF CAMx AND SMOKE/CMAQ ALGORITHMS	3-1
3.1 Setup and Input Conditions	3-1
3.2 Results and Summary	3-2
3.3 Issues Identified With SMOKE/CMAQ Algorithm	3-9
4. TESTING CAMX PLUME RISE UPDATES.....	4-1
4.1 Test Bed Setup and Results.....	4-2
4.2 Testing Plume Rise Algorithms in CAMx.....	4-7
5. CONCLUSIONS.....	5-1
5.1 Recommendations.....	5-2
6. REFERENCES.....	6-1

TABLES

Table 2-1. Comparison of important plume rise features for several models.....	2-1
Table 3-1. Meteorological conditions for the plume rise test bed	3-1
Table 3-2. Stack parameters for the plume rise test bed	3-2
Table 4-1. Meteorological conditions for the plume rise test bed	4-2

FIGURES

Figure 3-1. CAMx (blue bars) and SMOKE/CMAQ (yellow bars) plume rise for two tall/hot stack configurations (columns) and four stability regimes (rows). Each bar also shows the range of layers receiving emissions (black lines). Each individual plot shows results for three ambient wind speeds..... 3-3

Figure 3-2. CAMx (blue bars) and SMOKE/CMAQ (yellow bars) plume rise for two tall/cool stack configurations (columns) and four stability regimes (rows). Each bar also shows the range of layers receiving emissions (black lines). Each individual plot shows results for three ambient wind speeds..... 3-4

Figure 3-3. CAMx (blue bars) and SMOKE/CMAQ (yellow bars) plume rise for two short/hot stack configurations (columns) and four stability regimes (rows). Each bar also shows the range of layers receiving emissions (black lines). Each individual plot shows results for three ambient wind speeds..... 3-5

Figure 3-4. CAMx (blue bars) and SMOKE/CMAQ (yellow bars) plume rise for two short/cool stack configurations (columns) and four stability regimes (rows). Each bar also shows the range of layers receiving emissions (black lines). Each individual plot shows results for three ambient wind speeds..... 3-6

Figure 4-1. CAMx original (blue bars) and updated (yellow bars) plume rise for two tall/hot stack configurations (columns) and three stability regimes (rows). Each bar also shows the range of layers receiving emissions (black lines). Each individual plot shows results for three ambient wind speeds..... 4-3

Figure 4-2. CAMx original (blue bars) and updated (yellow bars) plume rise for two tall/cool stack configurations (columns) and three stability regimes (rows). Each bar also shows the range of layers receiving emissions (black lines). Each individual plot shows results for three ambient wind speeds..... 4-4

Figure 4-3. CAMx original (blue bars) and updated (yellow bars) plume rise for two short/hot stack configurations (columns) and three stability regimes (rows). Each bar also shows the range of layers receiving emissions (black lines). Each individual plot shows results for three ambient wind speeds..... 4-5

Figure 4-4. CAMx original (blue bars) and updated (yellow bars) plume rise for two short/cool stack configurations (columns) and three stability regimes (rows). Each bar also shows the range of layers receiving emissions (black lines). Each individual plot shows results for three ambient wind speeds..... 4-6

Figure 4-5. Hourly domain-wide peak NOx differences between two CAMx simulations of the TCEQ 2006 Houston modeling periods using the updated and original CAMx plume rise algorithm. Red circles highlight the hours shown in Figures 4-6 through 4-9 4-9

Figure 4-6. Domain-wide NOx differences during the hour of peak positive difference (top) and peak negative difference (bottom) during the June 2006 CAMx simulation using the updated and original CAMx plume rise algorithm 4-10

Figure 4-7. Domain-wide ozone differences for the same hours shown in Figure 4-6 during the June 2006 CAMx simulation using the updated and original CAMx plume rise algorithm. 4-11

Figure 4-8. Domain-wide NOx differences during the hour of peak positive difference (top) and peak negative difference (bottom) during the August-October 2006 CAMx simulation using the updated and original CAMx plume rise algorithm 4-12

Figure 4-9. Domain-wide ozone differences for the same hours shown in Figure 4-8 during the August-October 2006 CAMx simulation using the updated and original CAMx plume rise algorithm..... 4-13

Figure 4-10. NOx concentration profiles at selected hours during the June 2006 (top) and August-October 2006 (bottom) CAMx simulations. Results are shown using the original plume rise algorithm (blue) and updated algorithm (red). Morning profiles on the left show episode-peak positive surface NOx concentrations. Afternoon profiles on the right show episode-peak negative surface NOx concentrations..... 4-15

Figure 4-11. Ozone concentration profiles at selected hours during the June 2006 (top) and August-October 2006 (bottom) CAMx simulations. Results are shown using the original plume rise algorithm (blue) and updated algorithm (red). Dates and times are identical as Figure 4-10..... 4-16

EXECUTIVE SUMMARY

Plume rise from point source stacks depends upon the configuration of the stack, physical properties of the exiting gases, and the state of the ambient atmosphere. Air quality models adopt different approaches to calculate plume rise. The objectives of this project were to compare and evaluate plume rise algorithms in several models (CAMx, SMOKE/CMAQ, CALPUFF, AERMOD), and then to update CAMx with an improved point source plume rise algorithm. Our model review led us to recommend the SMOKE/CMAQ approach for consideration as an alternative option in CAMx. However, comparison of the CAMx and SMOKE/CMAQ plume rise calculations in a series of idealized tests revealed some undesirable features in the SMOKE/CMAQ plume rise calculations that led to counter-intuitive behavior across different wind speed and stability regimes. As a result, it was dropped from further consideration; the remainder of the project focused on improving the current CAMx plume rise algorithm and evaluating it via idealized tests and existing modeling applications. The idealized tests revealed that in most cases the original and updated plume rise estimates were identical, but results were improved for capping stable layer cases. In particular, the new capability to distribute plume mass vertically through several layers led to penetration into the capping inversion.

CAMx was run using the 2006 TCEQ Houston modeling database so that the plume rise impacts could be assessed over as many meteorological and geographical conditions as possible. Overall, surface NO_x differences tended to be small and negative, with peak differences remaining well within ± 10 ppb. The propensity toward NO_x decreases was mostly a result of spreading emissions over multiple layers, but occasionally higher plume estimates pushed more mass to higher layers above the mixing depth. In general, the plume rise update resulted in mostly NO_x reductions during daytime hours, while NO_x increases generally occurred during evening through early morning hours, periods of maximum stability. Plume spread and higher daytime rise modulated the amount of NO_x in the boundary layer, and this further impacted ozone profiles by altering the location and depth where ozone titration by fresh NO_x occurred. While our analyses show that formulation differences among plume rise algorithms do not lead to significant impacts for modeling secondary pollutants such as ozone and PM, the same may not be true for applications that focus on concentrations of primary emissions near sources (e.g., toxics) and associated human exposure.

1. INTRODUCTION

1.1 BACKGROUND

Plume rise from point source stacks depends upon the configuration of the stack, physical properties of the exiting gases, and the state of the ambient atmosphere. Air quality models adopt different approaches to calculate plume rise. For example, the Comprehensive Air quality Model with extensions (CAMx) calculates plume rise internally and determines a single layer in which to inject point source emissions. On the other hand, the Community Multi-scale Air Quality (CMAQ) model usually relies upon an external plume rise calculation performed by the Sparse Matrix Operator Kernel Emissions (SMOKE) processor, which distributes emissions vertically to multiple layers.¹

The objectives of this project were to compare and evaluate several approaches to calculate plume rise, and then to update CAMx with an improved point source plume rise algorithm. ENVIRON reviewed and compared the plume rise algorithms currently employed within the following widely-used air quality modeling systems:

- CAMx (ENVIRON, 2010);
- SMOKE/CMAQ (UNC, 2009; Byun and Schere, 2006);
- California Puff (CALPUFF) model (Scire et al., 2000);
- AERMOD Gaussian plume model (EPA, 2004).

We also investigated the plume rise calculation used within the Second-order Closure Integrated Puff (SCIPUFF) model and found that it reportedly uses the same plume rise algorithm as SMOKE/CMAQ (EPRI, 2000). We attempted to review the approach used in the new coupled meteorology-chemistry model, WRF-Chem (Peckham et al., 2009) but learned that the model relies on three-dimensional emission inputs, similar to older versions of CMAQ, for which the plume rise is determined externally. While the WRF-Chem user's guide states that it is expected that emission inputs are to be developed independently on a case-by-case basis, WRF-Chem is distributed with an example pre-processor (emiss_v03.F) that is hard-wired to generate emission inputs from the 2005 U.S. National Emission Inventory. According to the WRF-Chem user's guide:

“Currently no plume rise calculations directly couple WRF dynamics to anthropogenic point emissions. The emiss_v03.F routine includes some plume rise from the Brigg's formulation due to momentum lift from direct injection, and a specified horizontal wind climatology.”

Given that the WRF-Chem emissions pre-processor appears to be a temporary place-holder that contains a simple plume rise calculation, this algorithm was not considered further.

¹ Beginning with version 4.6, CMAQ includes the same SMOKE plume rise algorithm as an internal option.

Organization of this Report

Section 2 of this report summarizes and compares/contrasts the plume rise algorithms used in each of the models listed above. The summary of the individual approaches is qualitative with the focus on characterizing their similarities and differences with as little complication as possible. From this comparison, ENVIRON recommended more detailed investigation of the SMOKE/CMAQ plume rise algorithm as a potential alternative option in CAMx.

Section 3 documents a comparison of the CAMx and SMOKE/CMAQ plume rise calculations in a series of idealized tests covering a range of stack parameters and environmental conditions (the test bed). The comparisons revealed that in most conditions tested, the CAMx and SMOKE/CMAQ plume rise estimates were very similar. However, some undesirable features were apparent in the SMOKE/CMAQ plume rise calculations that led to counter-intuitive behavior across different wind speed and stability regimes.

Results of these tests were discussed with TCEQ and the SMOKE/CMAQ plume rise algorithm was dropped from consideration as an alternative to the CAMx plume rise algorithm. Instead, the remainder of the project focused on improving weaknesses of the current CAMx plume rise algorithm that were identified in Section 3. Section 4 describes the CAMx plume rise improvements, test bed comparisons of the updated CAMx algorithm, and CAMx modeling results using both the original and updated plume rise algorithms.

1.2 OVERVIEW OF PLUME RISE CALCULATIONS

In general, the plume rise algorithms used in modern grid (Eulerian) and plume-oriented (Lagrangian) air quality models are rooted in parameterized equations that were developed decades ago. These empirical relationships were constructed from experimental data for a variety of release and atmospheric conditions. The most commonly applied plume rise equations were first developed by Briggs (1969, 1971, 1972), and over the next decade or so various enhancements to these relationships were made to consider such effects as plume penetration into capping stable layers, downwash from stack tips and nearby structures, and multi-layer stability (e.g., Briggs, 1975, 1984; Turner, 1985; Turner et al., 1986; Weil, 1988, 1997).

Plume rise algorithms typically include equations that characterize the effluent's buoyancy and momentum as it exits the stack. From this, plumes can be characterized in three ways (Seinfeld and Pandis, 1998):

Buoyant plume:	Initial buoyancy >> Initial momentum
Forced plume:	Initial buoyancy ~ Initial momentum
Jet:	Initial buoyancy << Initial momentum

Separate buoyancy and momentum equations are employed for neutral, unstable and stable atmospheric conditions. Often plume rise is calculated from either buoyant flux or momentum flux with the choice of which to use based on which equation yields greater rise above the stack. Some models combine buoyant and momentum effects into single equations. In either case, the final rise is added to the stack height to determine the final total plume centerline height above the ground (referred to as "effective stack height").

2. SUMMARY OF PLUME RISE ALGORITHMS

This section summarizes and compares/contrasts the plume rise algorithms currently employed within the following widely-used air quality modeling systems:

- CAMx;
- SMOKE/CMAQ;
- CALPUFF;
- AERMOD.

The summary of the individual approaches is qualitative with the focus on characterizing their similarities and differences with as little complication as possible. Following this comparison, we recommended more detailed investigation of the SMOKE/CMAQ plume rise algorithm as a potential alternative option in CAMx.

Table 2-1 summarizes some of the key features of the plume rise algorithms used in each of the air quality models reviewed in this work. Details of each treatment are described below.

Table 2-1. Comparison of important plume rise features for several models.

	CAMx	SMOKE/ CMAQ	CALPUFF	AERMOD
Multi-layer rise	X	X		
Multi-layer injection		X	n/a	n/a
Considers capping stable layer	X	X	X	X
Partial penetration into capping stable layer		X	X	X
Vertical wind shear effects			X	
Stack tip downwash	X		X	X
Combines buoyant and momentum fluxes			X	X

2.1 CAMx

The CAMx plume rise algorithm is based on the multi-layer stability-dependent approach of Turner et al. (1986), which in turn has its roots in the original Briggs equations. The atmospheric stability in the model layer containing the stack top is first calculated to determine whether stable or neutral/unstable conditions exist at the point of release. Then momentum and buoyant fluxes are calculated from stack parameters using equations specific to the atmospheric stability. The larger of momentum or buoyancy rise is selected, and the other is disregarded.

If momentum rise is chosen, it is set as the final plume rise; thus in this case plume rise is entirely based on momentum exiting the stack and stability of the layer containing the stack; no further consideration is given to atmospheric conditions in layers above the stack. However, if buoyant rise is dominant then residual buoyancy flux is determined for each model layer above the stack until buoyant energy is dissipated. Residual buoyancy accounts for mixing with air as it traverses a given layer, and specific equations are used according to stability of the current layer. Therefore, buoyant rise considers the changing stability and wind conditions in each layer and thus will be impeded by a capping stable layer. The buoyant rise into the final layer containing zero residual buoyancy is taken as the final plume rise.

After final plume rise is determined, CAMx applies a stack tip downwash factor according to the Froude number (a relationship between wind speed and exit velocity). If the exit velocity is 50% larger than wind speed, no adjustment is made. If the exit velocity is smaller than the wind speed, downwash is overwhelming and there is no plume rise. In between these two extremes, a factor between 0 and 1 is linearly applied to the plume rise. All emissions are injected into the single grid cell in the column containing the stack, within the layer containing the final plume rise. Emissions are not distributed through multiple layers.

2.2 SMOKE/CMAQ

SMOKE has historically calculated time-dependent effective plume heights for point sources as part of its process of generating three-dimensional gridded emission inputs for the CMAQ photochemical model. Since the release of CMAQ v4.6, the photochemical model includes the option to calculate plume rise internally, in which case the SMOKE plume rise calculation is bypassed and SMOKE instead supplies pertinent stack information for each point source to CMAQ. The plume rise algorithms in SMOKE and CMAQ are identical.

As described by Houyoux (1998), SMOKE employs a multi-layer stability-dependent plume rise algorithm similar to CAMx. The approach in SMOKE is based on the algorithm first employed in the Regional Acid Deposition Model (RADM; Byun and Binkowski, 1991; Turner, 1985) with some important improvements. SMOKE distinguishes between three stability regimes (stable, neutral, and unstable) as opposed to the two regimes considered in CAMx (stable and neutral/unstable).

In general, the SMOKE plume rise algorithm operates very similarly to CAMx. Atmospheric stability at stack top is first determined, and then momentum and buoyant fluxes are calculated from stack parameters using equations specific to the three atmospheric stability regimes. If momentum rise dominates, then it is chosen and buoyant rise through layers above is disregarded. If buoyant rise dominates, then residual buoyancy flux is re-calculated using stability-dependent equations for each successive layer until zero residual is reached. SMOKE adds considerable complexity to this approach by explicitly considering mixing height in its stability classification, and this is used to determine partial plume penetration into the capping stable layer. Six different cases are possible, which consider the stack top height, stack top stability, and the mixing height. SMOKE does not include any stack tip downwash adjustments to final rise.

Unlike CAMx, SMOKE distributes plume emissions through potentially several layers, depending on plume rise and the six stack/mixing height cases described above. Once plume rise is determined, the top and bottom of the plume is set to 50% of the plume rise above and below the final plume rise, respectively (i.e., the depth of the plume equals the plume rise). Emissions are distributed to each layer within this depth according to the pressure in each layer (i.e., the distribution is weighted by atmospheric mass in each layer).

2.3 CALPUFF

The CALPUFF model determines plume rise from several types of sources, including point, buoyant line, and buoyant area. The basic point source plume rise equations are based on those

of Briggs (1975). Like CAMx, CALPUFF considers two stability regimes determined by surface-based meteorological conditions at the stack: stable and neutral/unstable. Although CALPUFF reads vertically resolved meteorological input data, the plume rise algorithm does not consider rise through multiple layers.

CALPUFF first calculates plume rise using formulas that combine momentum and buoyancy fluxes together; different equations are used for stable and neutral/unstable conditions. The rise equations include downwind horizontal distance traversed during the rise, a feature referred to as “transitional” plume rise. This is important for near-source plume models that are designed to explicitly treat plume dynamics at very short length scales. A minimum wind speed of 1 m/s is imposed during calm or low wind speed conditions. As in CAMx, CALPUFF treats the stack-tip downwash. The Froude number criteria and adjustment equations are very similar, except CALPUFF adjusts the stack height downward instead of adjusting the final plume rise value, which reduces the overall effective stack height.

During neutral/unstable conditions, plume rise can also penetrate into the capping stable layer above the mixing height if the initial plume rise calculation exceeds the mixing height. CALPUFF first calculates a penetration parameter and the fraction of the plume remaining in the mixed layer. Based on these variables, two different plume rises are determined (above the mixing height and below); the penetrating rise is then used to sequester puff mass in the capping stable layer from mixing downward to the ground. It is not clear from the documentation if the penetrating mass fraction is split into a different puff, or if a single puff is simulated but only a fraction of mass is available for mixing.

The plume rise by buoyant flux can also be reduced when there is a vertical wind shear above the stack top. Scire et al. (2000) state that for most medium to tall stacks well above the surface shear layer (~50 m) these effects are unimportant. However this effect cannot be ignored for shorter stacks. CALPUFF includes stable and neutral/unstable buoyant rise equations for short stacks that include a power law relationship of wind with respect to the height. For these stacks, the minimum among shear-based rise, downwash-adjusted rise, and the initial non-shear rise is taken for the final plume rise.

2.4 AERMOD

The plume rise algorithm within the AERMOD model has several common features with CALPUFF. It is based on historical schemes (e.g., Briggs, 1975, 1984; Weil, 1988) but includes numerous updates to account for such phenomena as downwash, transitional rise, and plume penetration above the mixing height (e.g., Weil et al., 1997). While meteorological data at multiple vertical levels are available to AERMOD, its plume rise algorithm is not a multi-layer scheme. Local stability at stack top is used to decide which plume rise equation is used.

The model uses input vertical profiles of meteorological data to extract wind speed and temperature gradient at the stack top for the momentum and buoyant flux calculations. Within the convective boundary layer (equivalent to the neutral/unstable cases in other models), the plume rise equation is a combination of momentum and buoyant fluxes as in CALPUFF (Briggs, 1984). In the stable boundary layer (equivalent to the stable case), the plume rise equation is also a combination of momentum and buoyant fluxes according to the equations of Weil (1988). Both rise equations include downwind horizontal transport for transitional plume rise.

Adjustments are made in the case of near-neutral stability and near-calm conditions (which can both lead to unrealistically large plume rise according to the authors).

AERMOD also uses mixing height information similarly to CALPUFF; if stacks are located above the mixing height, it uses equations corresponding to stable conditions, even if the surface is unstable. AERMOD also considers the possibility that plumes penetrate into the capping stable layer above the mixing height, and corrects plume rise in such cases. The mass that has penetrated into the capping layer is assigned to a virtual source and treated separately. Also, AERMOD employs the same stack-tip downwash adjustment as CALPUFF. However, AERMOD does not include any wind shear effects.

2.5 ORIGINAL RECOMMENDATION FOR CAMx

The purpose of this review was to compare/contrast the features of each of the plume rise algorithms employed within today's most widely used modeling systems. From this review, we developed a recommendation for which approach would best serve as an alternative option in CAMx.

Given the vastly different spatial frames between the Eulerian grid and Lagrangian plume forms, and their intended purpose, certain capabilities or advantages offered in the Lagrangian model plume rise algorithms may not be important for the Eulerian models, or even appropriate or applicable (e.g., the concept of "transitional" rise is useless in grid models in which emissions are instantly emitted/diluted into grid cell volumes). One feature that CALPUFF possesses over all other algorithms is that it accounts for the effects of wind shear near the ground (a separate effect from stack-tip downwash, which is caused by the physical wake effect of the stack on plume dynamics). However, we are not convinced that this would provide a substantial advantage for Eulerian models with discrete, fairly thick layers. The most important advantage offered by the CAMx and SMOKE/CMAQ algorithms is the use of multi-layer meteorological conditions that independently control buoyant plume rise according to the local stability profile. However, both grid model approaches use older rise equations that separately choose between momentum and buoyancy flux, while the Lagrangian models combine these fluxes into a single rise equation.

In the Eulerian models, the residual buoyancy flux into each successive layer was formulated for the specific buoyancy equations employed. If one of the Lagrangian algorithms were to be adapted to a multi-layer technique in CAMx, it would be necessary to derive or approximate the residual flux, and this would require specialized knowledge of decades-old derivation and empirical techniques used for the original Briggs (1975) equations. This was clearly not within the intended scope of this project.

Therefore, our recommendation focused on the SMOKE/CMAQ approach. This algorithm does offer two advantages (for a single reason) over the current CAMx scheme: (1) distribution of emissions mass through multiple layers; and (2) as a result, possible partial plume penetration into capping stable layers above the mixing height according to six cases related stack height and mixing height. However, we were concerned about the assumptions that plume depth equals plume rise, and that emissions are distributed uniformly through this depth (albeit weighted by pressure, which would not be significant in most cases). There is no clear reference given in the SMOKE documentation to support these otherwise arbitrary assumptions, although we later learned that this is a common "rule-of-thumb" that has historically been applied for plume

models (Turner and Schulze, 2007). Especially under stable conditions, this approach could bias the model toward over-dilution of the emissions (beyond the inherent horizontal dilution from injecting emissions into grid volumes). Conversely, we also recognize that it is not always valid to assume that emissions are injected into the single layer containing final plume rise (the CAMx approach).

The project scope called for adapting the alternative plume rise option for both grid injection and PiG injection. The PiG model contains an equation from SCIPUFF (EPRI, 2000) that explicitly accounts for plume spread as it rises due to entraining ambient air, and thus use of the SMOKE/CMAQ vertical emissions distribution would not be appropriate for PiG. Instead, we decided to use the PiG plume spread equation to ultimately replace the vertical distribution assumption in the SMOKE/CMAQ algorithm.

3. COMPARISON OF CAMx AND SMOKE/CMAQ ALGORITHMS

This section presents a comparison of CAMx and SMOKE/CMAQ plume rise calculations from a series of idealized tests covering a range of stack parameters and environmental conditions. These tests were conducted using a stand-alone “test bed” external to CAMx that defines each test scenario and runs each of the algorithms. This approach enabled quantitative comparisons of the CAMx and SMOKE/CMAQ algorithms and also resulted in a CAMx-ready version of the SMOKE/CMAQ algorithm that could be implemented directly into CAMx.

3.1 SETUP AND INPUT CONDITIONS

A stand-alone test bed was developed to compare CAMx and SMOKE/CMAQ plume rise algorithms for a set of idealized conditions. Various meteorological conditions and stack configurations were considered. The test bed was set up to define vertical profiles of meteorological variables through a single column of 40 vertical layers, each 50 m deep (2000 m total depth). Surface temperature and pressure were set to 298 K (25 °C) and 1013.25 mb (1 atm), respectively. Four stability classes were considered: stable, neutral, unstable, and unstable with a stable capping layer at 500 m (Table 3-1). For each stability case, three wind speeds were considered: 1, 5, and 10 m/s. The pressure profile was determined from the hydrostatic equation according to the temperature profile.

Table 3-1. Meteorological conditions for the plume rise test bed.

	Surface temperature	298 K	
	Surface pressure	1013.25 mb	
	Surface roughness	1 m	
	Constant wind profile	1, 5, 10 m/s	
Stability Class	Temperature lapse rate (K/km)	Potential Temp. lapse rate (K/km)	mixing height (m)
stable	-5	5	25
neutral	-10	0	2000
unstable	-12	-2	2000
capping	-12 / -5	-2 / 5	500

An explicit mixing height is needed for the SMOKE/CMAQ algorithm, which may be difficult to specify in situations where the atmosphere has complex vertical structure, e.g., coastal environments, but was easily specified for the simple scenarios evaluated here. For the stable case, 25 m was used; for the neutral and unstable cases, 2000 m was used; for the capping case, 500 m was used to coincide with the changing temperature gradient at that altitude. The SMOKE/CMAQ algorithm also needs a surface friction velocity, which is a micro-meteorological parameter that characterizes the amount of turbulent momentum flux within the surface layer (i.e., lowest ~50 m of the atmosphere). Friction velocity was calculated within the test bed using a CAMx routine that employs the stability-dependent parameterization of Louis (1979). An urban surface roughness of 1 m was assumed.

Eight different stack configurations were considered that varied stack height/diameter, effluent temperature, and exit velocity (Table 3-2). Tall stacks were 100 m high and 5 m wide, while

short stacks were 10 m tall and 1 m wide. Hot stacks were 450 K (177 °C), while cool stacks were 320 K (47 °C). Fast stacks were 20 m/s, while slow stacks were 1 m/s. A total of 96 cases were run to compare the CAMx and SMOKE/CMAQ plume rise algorithms: 4 stabilities × 3 winds × 8 stacks.

Table 3-2. Stack parameters for the plume rise test bed.

Stack #	Height, Diameter (m)	Temperature (K)	Velocity (m/s)
1	100, 5	450	20
2	100, 5	450	1
3	100, 5	320	20
4	100, 5	320	1
5	10, 1	450	20
6	10, 1	450	1
7	10, 1	320	20
8	10, 1	320	1

3.2 RESULTS AND SUMMARY

Figures 3-1 through 3-4 present bar charts comparing CAMx and SMOKE/CMAQ total effective stack height (i.e., stack height + plume rise) for all eight stack cases. Figure 3-1 shows results for the tall/hot stacks, Figure 3-2 shows results for the tall/cool stacks, Figure 3-3 shows results for the short/hot stacks, and Figure 3-4 shows results for the short/cool stacks. In each individual plot, three wind speed cases are shown side-by-side. Columns of plots vary exit velocity (fast on the left, slow on the right). Rows of plots are arranged by atmospheric stability. To evaluate differences in emission injection, the plume rise bars are annotated to show the layer ranges, or vertical depths, that receive the emissions (vertical black lines).

Analysis of Plume Rise

The following observations were made from these comparisons.

In most cases, CAMx and SMOKE/CMAQ plume rise estimates are very similar.

With a few exceptions as discussed below, most combinations of meteorology and stack configuration result in very similar effective stack height. These small differences in plume rise will tend to result in the CAMx and SMOKE/CMAQ plume centers being placed in the same layers (note that we will later discuss the ramifications of vertically distributing the emission injection).

Plume rise is mostly insensitive to neutral vs. unstable cases.

For a given stack configuration, CAMx results for neutral and unstable cases are identical because only a single set of equations are used for neutral/unstable conditions. Furthermore, CAMx results are usually the same for unstable and capping cases except for fast stacks at slow

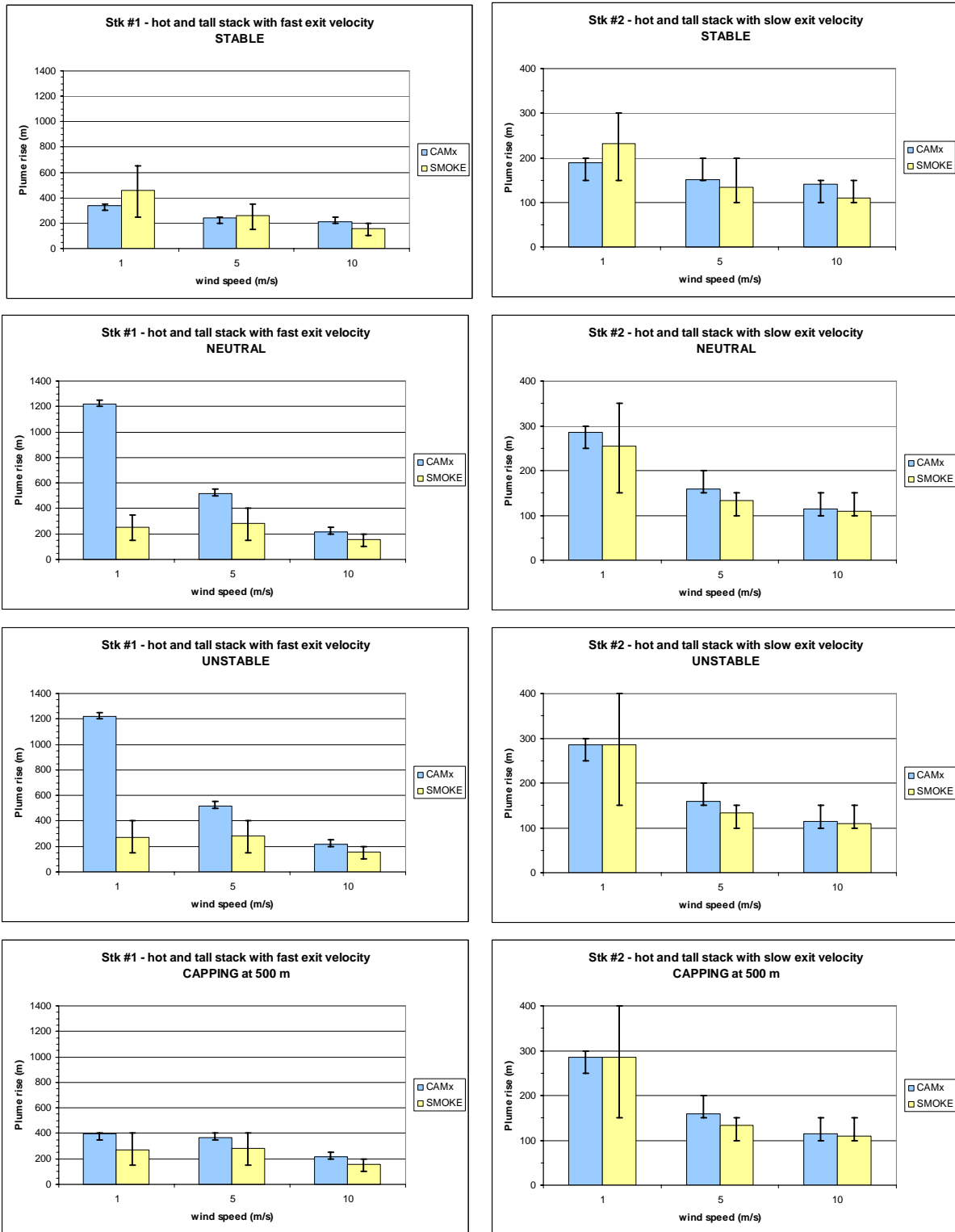


Figure 3-1. CAMx (blue bars) and SMOKE/CMAQ (yellow bars) plume rise for two tall/hot stack configurations (columns) and four stability regimes (rows). Each bar also shows the range of layers receiving emissions (black lines). Each individual plot shows results for three ambient wind speeds.

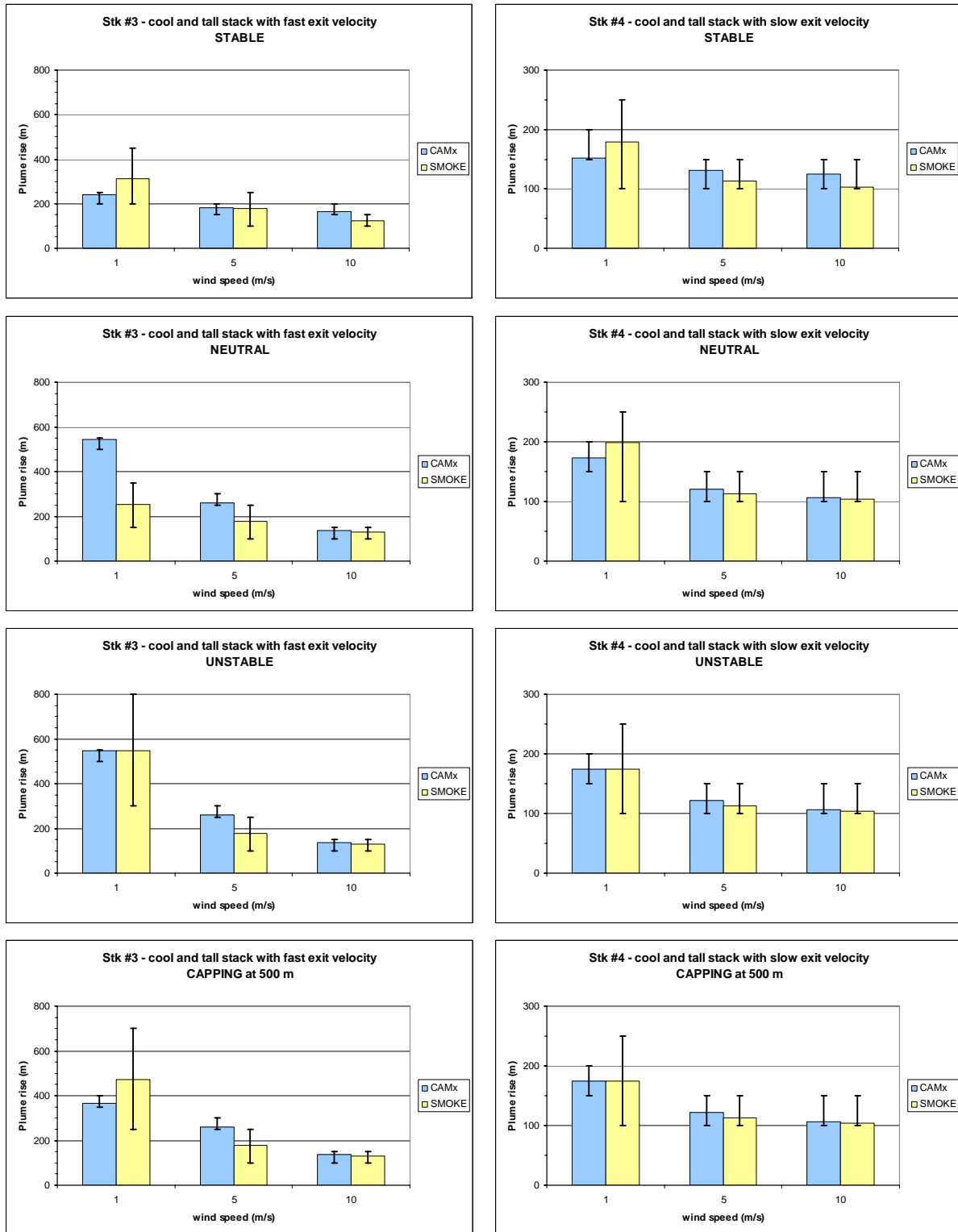


Figure 3-2. CAMx (blue bars) and SMOKE/CMAQ (yellow bars) plume rise for two tall/cool stack configurations (columns) and four stability regimes (rows). Each bar also shows the range of layers receiving emissions (black lines). Each individual plot shows results for three ambient wind speeds.

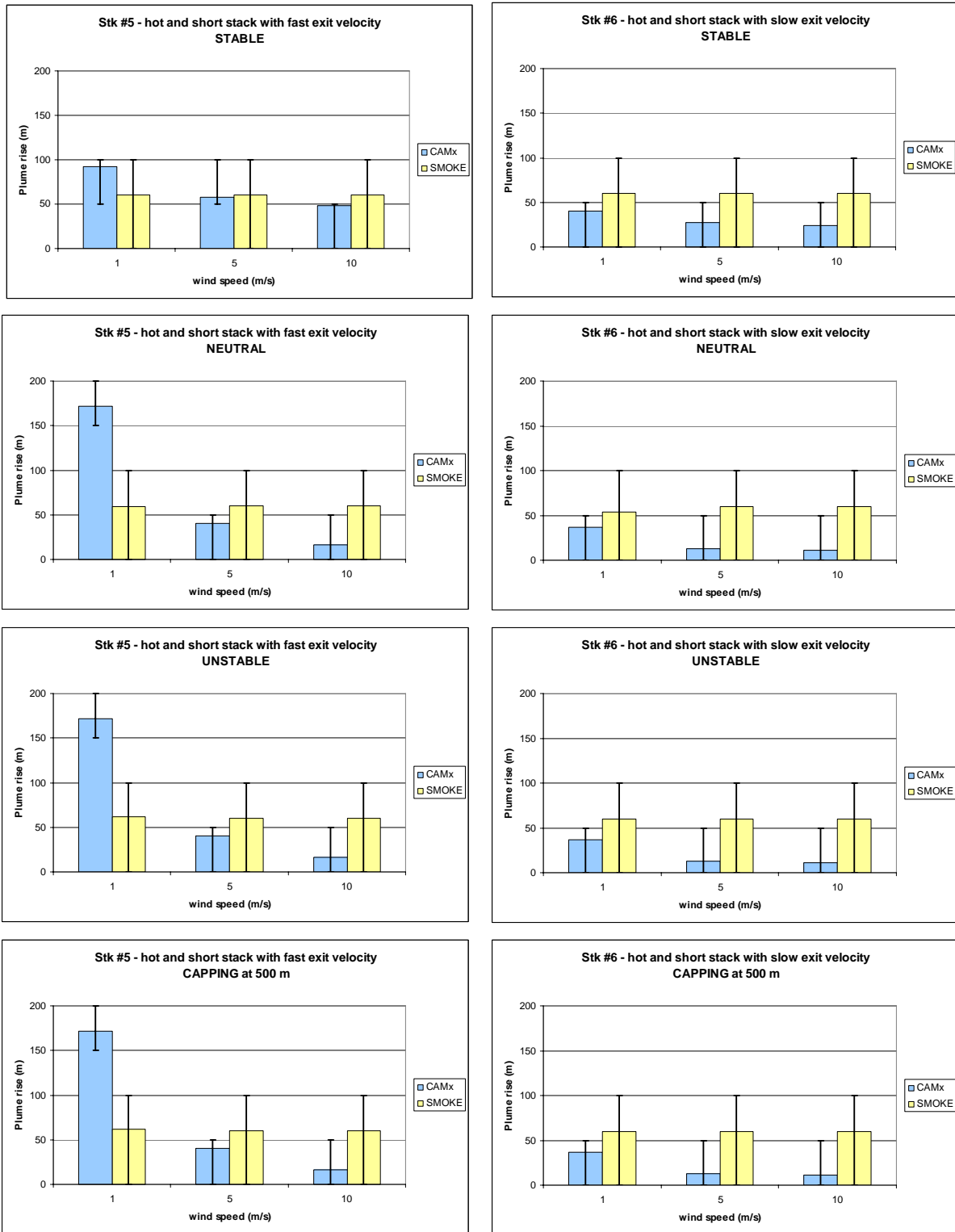


Figure 3-3. CAMx (blue bars) and SMOKE/CMAQ (yellow bars) plume rise for two short/hot stack configurations (columns) and four stability regimes (rows). Each bar also shows the range of layers receiving emissions (black lines). Each individual plot shows results for three ambient wind speeds.

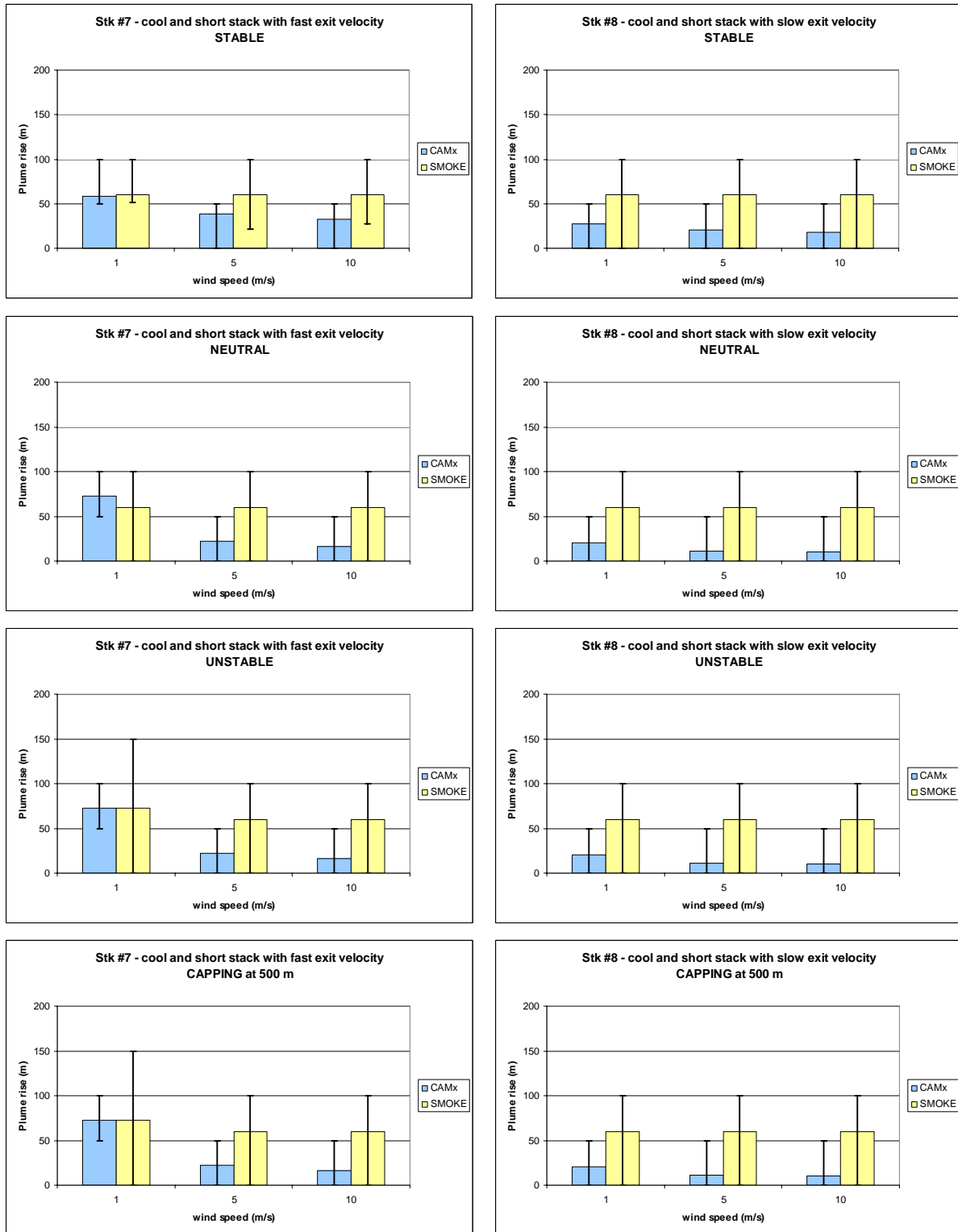


Figure 3-4. CAMx (blue bars) and SMOKE/CMAQ (yellow bars) plume rise for two short/cool stack configurations (columns) and four stability regimes (rows). Each bar also shows the range of layers receiving emissions (black lines). Each individual plot shows results for three ambient wind speeds.

wind speeds. This is because in most cases with winds greater than 1 m/s, plume rise stops well short of 500 m. SMOKE/CMAQ results are also similar between neutral and unstable conditions for wind speeds of 5 and 10 m/s, but can be much different for light winds (1 m/s).

Interestingly, we find that in the unstable low-wind (1 m/s) case, SMOKE/CMAQ with the tall/cool/fast stack (stack #3) generates a much higher plume rise (475 m vs. 250 m) than the tall/hot/fast stack (stack #1). This result is counter-intuitive, but review of the code reveals why this occurs. The SMOKE/CMAQ algorithm considers both neutral and unstable buoyant plume rise under unstable conditions, chooses the smaller of the two, and resets the stability according to that selection. This overriding approach affects the calculation of residual buoyancy flux: the cool stack resulted in higher residual flux than the hot stack, resulting in higher plume rise for the cool stack.

CAMx plume rise can be much higher than SMOKE/CMAQ for neutral/unstable light wind conditions.

The only major difference between the CAMx and SMOKE/CMAQ plume rises (in terms of centerline plume height) occurs under light wind neutral/unstable conditions, with CAMx resulting in much higher plume rise (~1200 m) than SMOKE/CMAQ (~250 m) for hot/fast stacks. In fact, the neutral/unstable SMOKE/CMAQ rise is lower than its stable rise for the same stack and wind conditions. The reason why SMOKE/CMAQ squelches plume rise under these conditions is described in the paragraph above. Again, these particular conditions should maximize plume rise according to our conceptual perceptions.

CAMx plume rise is always much lower than the capping stable layer at 500 m.

When a capping stable layer is introduced, we expected the very high plume rise for the hot/fast stack under unstable conditions (~1200 m) to be reduced to about 500 m. But CAMx plume rise never exceeds ~400 m in the capping condition. We traced this effect to the fact that CAMx calculates plume *centerline rise* in neutral/unstable conditions, but calculates plume *top rise* for any stable layers aloft; thus in the stable capping layer, the plume *centerline* is taken as 2/3 the rise of the *top*, resulting in an additional plume rise reduction.

SMOKE/CMAQ algorithm is insensitive to stack or meteorological conditions for short stacks.

For the short stacks in Figures 3 and 4, SMOKE/CMAQ sets most plume rise to 60 m. This is because SMOKE/CMAQ does not allow point source plume centerlines to exist in the first layer. In most cases, the short stacks do not rise above the top of the first layer (50 m), and so SMOKE/CMAQ sets plume rise to two-thirds of the middle of the second layer and adds the stack height (60 m). This appears to result in a consistent upward bias for short stacks.

Analysis of Emissions Injection

The plume rise calculation is only part of the differences between the CAMx and SMOKE/CMAQ algorithms. While CAMx injects all emissions into the layer containing the plume centerline, SMOKE/CMAQ injects emissions into all layers containing the bottom through top of the plume. This can be a more significant difference between the two models than plume rise alone. A widely applied “rule-of-thumb” (Turner and Schulze, 2007) is adopted within SMOKE/CMAQ to determine the plume bottom and top. The bottom and top of the

plume are assumed to exist at 50% of the plume rise below and above the centerline, respectively. If this depth spans only one layer, that layer receives all emission mass. If this depth spans several layers, then fractions of the emissions are injected into these layers according to the fraction of plume depth extending into those layers. The distribution of emissions over layers is also weighted by pressure so that the emissions injection tends to result in a constant perturbation in mixing ratio rather than concentration.

The effect of the “rule-of-thumb” plume injection algorithm employed by SMOKE/CMAQ is to increase the vertical range of emission injection in direct proportion to the plume rise. Therefore, only single injection layers occur for the smallest plume rises, and CAMx and SMOKE/CMAQ algorithms agree most closely for the stack/meteorology configurations that result in minimal plume rise. Note that in stable cases where SMOKE/CMAQ has appreciable rise (e.g., stack #1, stable case in the upper left corner of Figure 1), the algorithm spread emissions through layers spanning 250-650 m, while CAMx placed emission in the single layer spanning 300-350 m. For short stacks (Figures 3 and 4), SMOKE/CMAQ consistently spread emissions through 0-100 m regardless of the stack/meteorological configuration, while CAMx placed emission either into the surface layer (0-50 m) or the second layer (50-100 m) depending on stack/meteorological conditions.

3.3 ISSUES IDENTIFIED WITH SMOKE/CMAQ ALGORITHM

The test bed comparisons revealed that in most conditions tested, the CAMx and SMOKE/CMAQ plume rise estimates were very similar. However, some undesirable features were identified in the SMOKE/CMAQ plume rise calculations that led to counter-intuitive behavior across different wind speed and stability regimes. These issues are summarized below:

- The algorithm considers six different regimes (defined by stability, winds, and the relation among stack height and mixing height) through a complex logical branching structure when choosing a plume rise equation to apply. This leads to very discontinuous and often unexpected behavior as meteorological conditions cross internally defined thresholds. In one extreme example, a hot/fast stack resulted in lower plume rise than a cool/fast stack under neutral stability, low wind conditions.
- Related to the above, the algorithm results in lower plume rise under unstable/neutral conditions than stable conditions. All other things being equal, plume rise should be higher under unstable than stable conditions (or at least the same).
- The algorithm is insensitive to stack or meteorological conditions for short stacks because it does not allow point source plume centerlines to exist in the first layer. If plume rise does not exceed the depth of the first layer, it sets plume rise to two-thirds of the middle of the second layer, which can result in a consistent upward bias for short stacks.
- The algorithm adopts a widely applied “rule-of-thumb” (Turner and Schulze, 2007) that plume depth equals plume rise when distributing mass to multiple model layers. It is difficult to believe that this rule of thumb applies uniformly in all conditions.
- An explicit mixing height is needed for the SMOKE/CMAQ algorithm, which may be difficult to specify in situations where the atmosphere has complex vertical structure, e.g., coastal environments.

Results of these tests were discussed with TCEQ and the SMOKE/CMAQ plume rise algorithm was dropped from consideration as an alternative to the CAMx plume rise algorithm. Instead, the remainder of the project focused on improving weaknesses of the current CAMx plume rise algorithm that were identified in these test-bed experiments. Results are presented in the next section.

4. TESTING CAMx PLUME RISE UPDATES

In this Section, we describe improvements to the CAMx plume rise algorithm and present comparisons between the original and updated routines. Comparisons were performed using the test bed described in Section 3 and CAMx modeling databases for the eastern U.S. developed by the TCEQ for the Houston-Galveston-Brazoria (HGB) State Implementation Plan (SIP).

Based on the results presented in Section 3, we implemented three specific modifications to the current CAMx plume rise algorithm:

1. Apply a lower limit to ambient wind speed (1 m/s minimum) to eliminate unrealistically large momentum and buoyancy rise under neutral/unstable light wind conditions;
2. Improve the layer-to-layer transition between neutral/unstable centerline rise to stable plume top rise that was leading to an artificial reduction in plume rise (particularly important for capping inversion cases);
3. Incorporate an algorithm to determine plume depth at final rise to allow for multi-layer plume injection, using diffusion equations from the PiG sub-model (i.e., not the “rule-of-thumb” approach of SMOKE/CMAQ).

Modifications (2) and (3) lead to improved plume emissions injection into the vertical layer structure plus partial plume penetration into a capping inversion.

The following equations were used to define the plume depth after reaching final rise (update #3). These are based on the approach used in the SCIPUFF model (EPRI, 2000) and were developed for use in the CAMx plume-in-grid (PiG) submodel. The plume depth D_p at final rise is given by

$$D_p = 3 \left(2 D_s^2 + 2 K t \right)^{1/2}$$

where D_s is stack diameter, K is plume diffusivity during rise, and t is the time of rise. The time of rise is determined by dividing final plume rise by the mean plume rise speed V_p , which is set to half the stack exit velocity. A lower limit of 1 m/s is applied to the exit velocity, so the minimum value of V_p is 0.5 m/s. The plume diffusivity is determined by the initial plume width (according to stack diameter) and the turbulent flux moment q_p^2 :

$$K = 0.15 \left(\sqrt{2} D_s \right) \sqrt{q_p^2}$$

where

$$q_p^2 = f_p V_p^2 \left[0.4 + \left(\frac{3v^2}{v^2 + V_p^2} \right) \right]$$

The turbulent flux moment is a function of the mean plume rise speed V_p , the ambient wind speed v taken at the level of final rise, and a plume entrainment coefficient f_p :

$$f_p = 1 + 4(\sqrt{2} D_s) g \left(\frac{T_p - T}{TV_p^2} \right)$$

where g is the gravitational constant ($9.8 \text{ m}^2/\text{s}$), T is ambient temperature at the level of final rise, and T_p is the mean plume temperature, taken as the mean of the stack exit temperature and the ambient temperature at final rise.

4.1 TEST BED SETUP AND RESULTS

The stand-alone test bed that we developed to compare CAMx and SMOKE/CMAQ plume rise calculations was used to compare the original and updated CAMx plume rise algorithms for the same set of idealized conditions. The test bed was set up identically as described in Section 3 with a few exceptions. Only three stability classes were considered: stable, neutral/unstable¹, and neutral/unstable with a stable capping layer at 500 m (Table 4-1). The CAMx algorithm does not explicitly require a “mixing height” parameter, as it diagnoses changes in stability from the layer-to-layer change in the temperature profile; nor does it require surface roughness.

Table 4-1. Meteorological conditions for the plume rise test bed.

	Surface temperature	298 K	
	Surface pressure	1013.25 mb	
	Surface roughness	N/A	
	Constant wind profile	1, 5, 10 m/s	
Stability class	Temperature lapse rate (K/km)	Potential Temp. lapse rate (K/km)	Mixing height (m)
Stable	-5	5	N/A
Neutral/unstable	-12	-2	N/A
Capping	-12 / -5	-2 / 5	N/A

Eight different stack configurations were considered that varied stack height/diameter, effluent temperature, and exit velocity (see Table 3-2). A total of 72 cases were run to compare the original and updated CAMx plume rise algorithms: 3 stabilities \times 3 winds \times 8 stacks.

Figures 4-1 through 4-4 present bar charts comparing original and updated CAMx total effective stack height (i.e., stack height + plume rise) for all eight stack cases. Figure 4-1 shows results for the tall/hot stacks, Figure 4-2 shows results for the tall/cool stacks, Figure 4-3 shows results for the short/hot stacks, and Figure 4-4 shows results for the short/cool stacks. In each individual plot, three wind speed cases are shown side-by-side. Columns of plots vary exit velocity (fast on the left, slow on the right). Rows of plots are arranged by atmospheric stability. To evaluate differences in emission injection, the plume rise bars are annotated to show the layer ranges, or vertical depths, that receive the emissions (vertical black lines).

¹ Recall that the CAMx algorithm employs the same equations for neutral and unstable conditions.

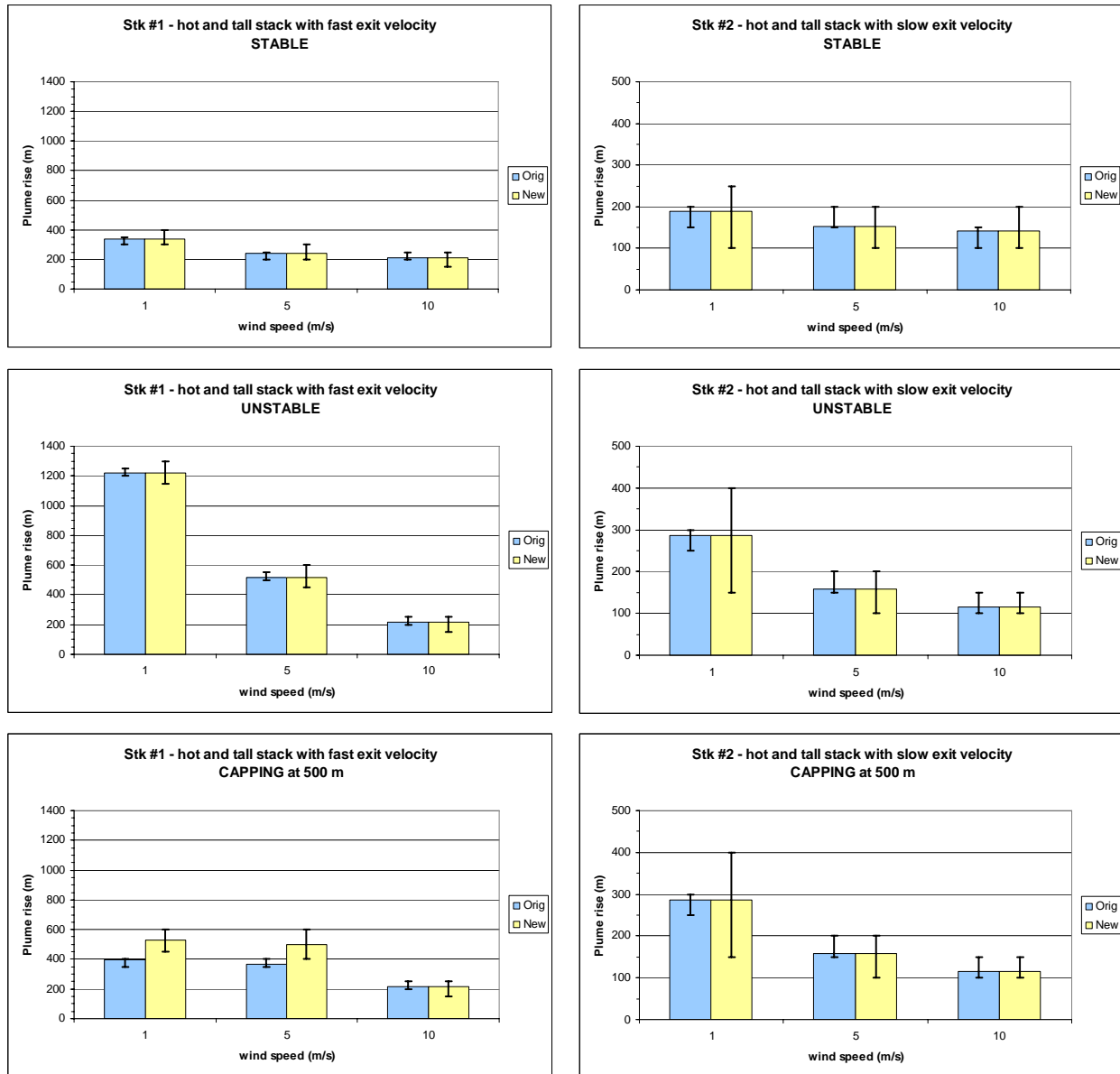


Figure 4-1. CAMx original (blue bars) and updated (yellow bars) plume rise for two tall/hot stack configurations (columns) and three stability regimes (rows). Each bar also shows the range of layers receiving emissions (black lines). Each individual plot shows results for three ambient wind speeds.

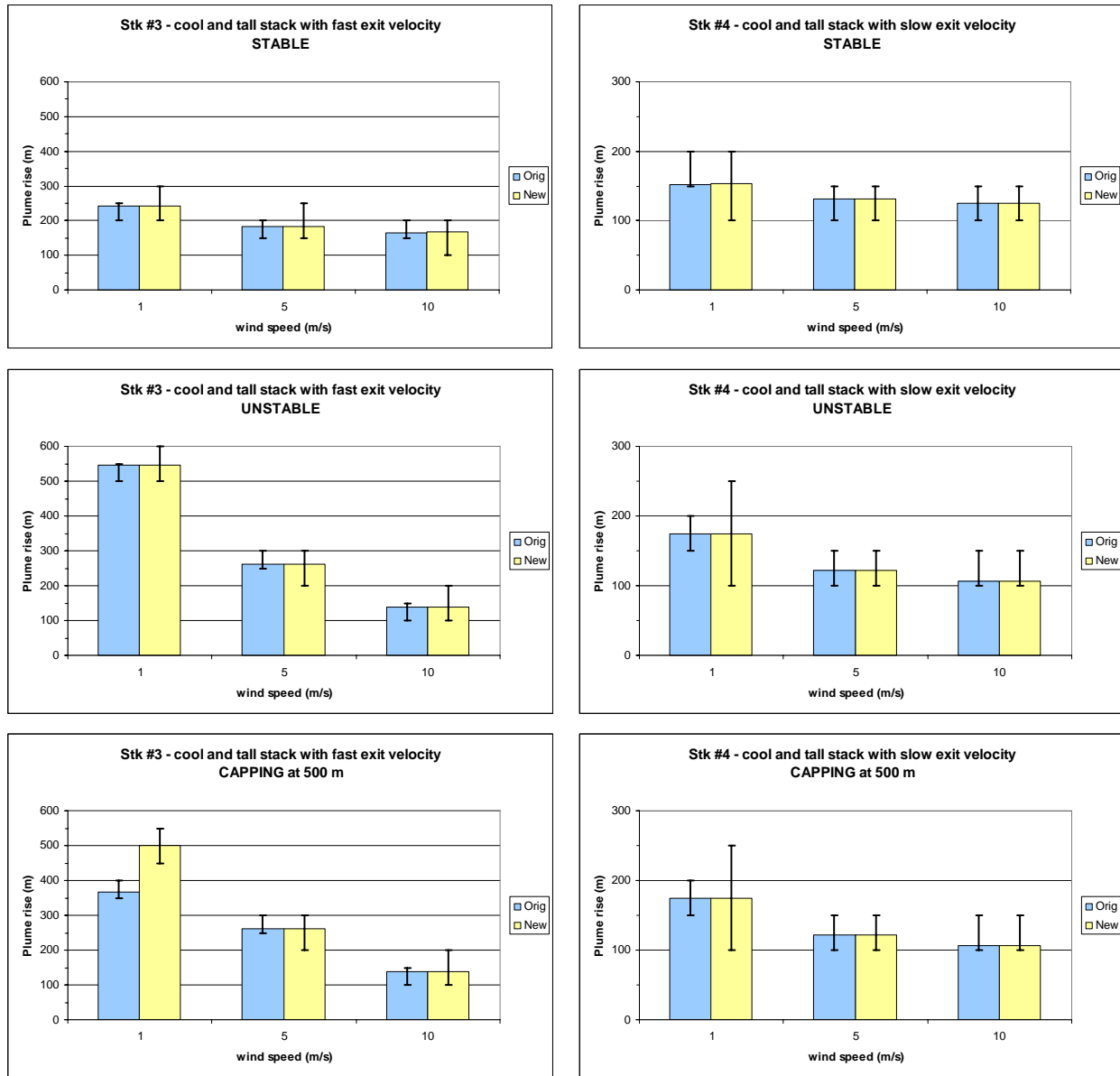


Figure 4-2. CAMx original (blue bars) and updated (yellow bars) plume rise for two tall/cool stack configurations (columns) and three stability regimes (rows). Each bar also shows the range of layers receiving emissions (black lines). Each individual plot shows results for three ambient wind speeds.

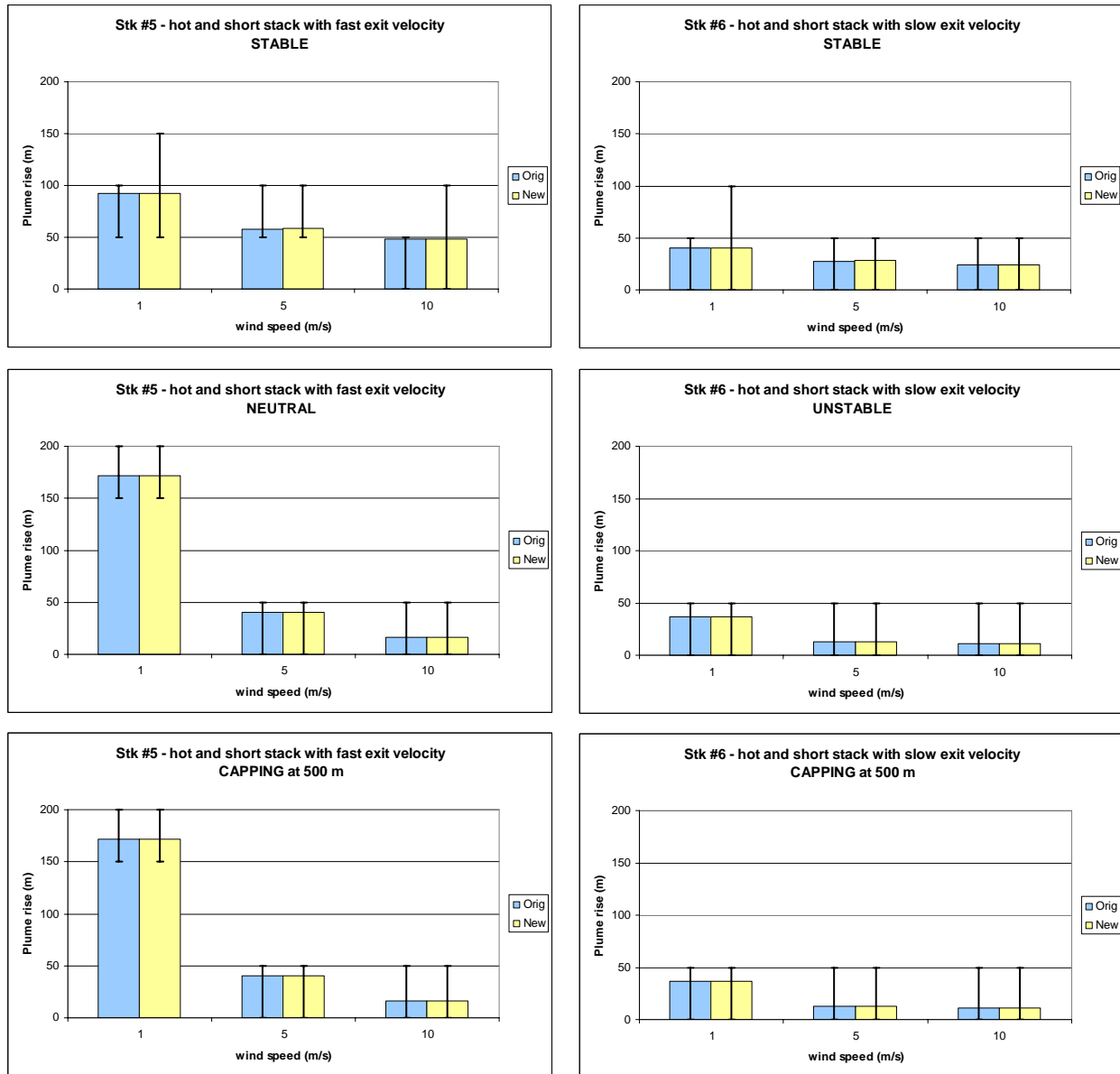


Figure 4-3. CAMx original (blue bars) and updated (yellow bars) plume rise for two short/hot stack configurations (columns) and three stability regimes (rows). Each bar also shows the range of layers receiving emissions (black lines). Each individual plot shows results for three ambient wind speeds.

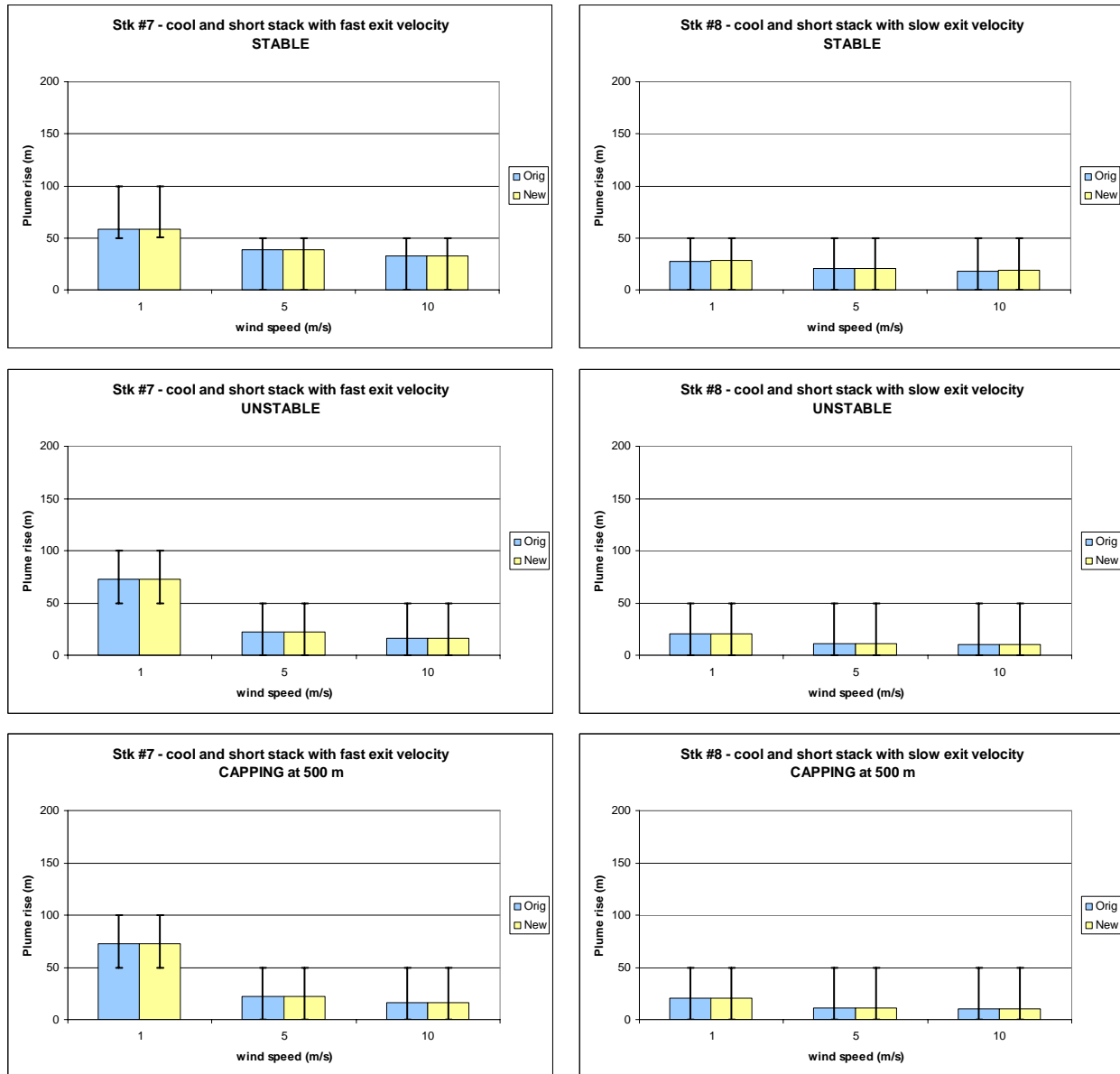


Figure 4-4. CAMx original (blue bars) and updated (yellow bars) plume rise for two short/cool stack configurations (columns) and three stability regimes (rows). Each bar also shows the range of layers receiving emissions (black lines). Each individual plot shows results for three ambient wind speeds.

The following observations were made from these comparisons.

In most cases, the original and updated plume rise estimates are identical.

As expected, and with a few exceptions as discussed below, most combinations of meteorology and stack configuration result in very similar effective stack height. This behavior will tend to result in the plume centers being placed in the same layers (note that we will later discuss the ramifications of vertically distributing the emission injection).

The updated plume rise is improved with a capping stable layer at 500 m.

When a capping stable layer is introduced, the plume rise for the hot/fast stack under neutral/unstable conditions (~1200 m) decreases substantially. The original algorithm reduces plume rise to 400 m. The improvements made to the code to better handle the transition from neutral/unstable to stable layers result a more expected outcome: the updated plume rise is reduced to just above 500 m. Improved results for the capping case are seen for all stack and wind conditions in which un-capped neutral/unstable rise is above 500 m.

The updated plume rise results in deeper mass injection.

The original CAMx algorithm injects all emissions into the layer containing the plume centerline, while the updated version injects emissions into all layers containing the bottom through top of the plume. With the introduction of the SCIPUFF plume spread equations from the PiG routine, plume depth is now determined as a function of stack diameter, plume temperature, plume velocity, time of plume rise, and ambient wind and temperature conditions. A uniform mass distribution through plume depth is assumed. If this depth is contained within a single layer, that layer receives all emission mass. If this depth spans several layers, then fractions of the emissions are injected into these layers according to the fraction of plume depth spanning those layers. We apply the “rule-of-thumb” that plume depth equals plume rise as a maximum limit.

In many cases, the emissions injection depth is similar to the original algorithm, especially for the short stacks that have smaller plume rise. The plume depths tend to be much deeper (up to 5 layers, or 250 m in this test bed) for stacks with slow exit velocities since plumes take longer to reach final rise than emissions from the fast stacks. Note that in some capping cases the plumes will extend or “penetrate” into the capping inversion.

4.2 TESTING PLUME RISE ALGORITHMS IN CAMx

The updated plume rise algorithm was incorporated into CAMx version 5.20. ENVIRON obtained the TCEQ 2006 Houston modeling datasets for the May 31 – June 15 and August 13 – October 11 simulation periods. These Houston modeling datasets employ a system of nested grids ranging from 4-km grid spacing in the Houston area, to 12-km spacing over the south-central U.S., to 36-km spacing over the entire eastern U.S. CAMx v5.20 was run for both periods over the full eastern U.S. domain using the original and updated plume rise routines so that the impacts could be assessed over as many meteorological and geographical conditions as possible. Since point source effects on grid concentrations are resolution-dependent, we ran these plume rise tests using the single 36-km eastern U.S. grid so that concentration differences could be assessed and compared on a consistent basis throughout the modeling domain.

Resulting CAMx surface concentration difference fields (new vs. original plume rise) for NO_x were screened over the entire modeling period, and specific grid columns were identified that contained the largest surface concentration impacts. Vertical NO_x and ozone concentration profiles for the selected grid columns were then compared for the standard and updated plume rise cases to evaluate changes in plume rise and depth. Several examples are described below.

Figure 4-5 shows the hourly domain-wide peak surface NO_x concentration differences during the June and August-October 2006 modeling periods. Overall, peak NO_x differences tend to be small and negative (around -1 to -2 ppb), with some peaks extending from less than -8 ppb to over +3 ppb. The largest differences are associated with some of the largest NO_x point sources. The fact that these peak differences are weighted toward lower NO_x surface concentrations suggests that the plume rise update tends to lead toward either higher rise or more dilution by spreading emissions over multiple layers. Generally, peak differences during June 2006 are roughly half the peak differences during August-October 2006. This may be due to the more quiescent and stable conditions that are more common during autumn months.

Hourly surface NO_x and ozone concentration difference fields on the 36-km grid were animated over the entirety of each episode to identify patterns and trends. Figures 4-6 through 4-9 show examples of NO_x and ozone from this animation at specific hours when the largest NO_x differences occurred in the time series of Figure 4-5 (noted by the red circles). In general, the plume rise update results in mostly NO_x reductions during daytime hours; again this agrees with our conceptual model that the updates result in higher plume rise and more NO_x dispersion from multi-layer injection. NO_x increases generally occurred during evening through early morning hours, periods of maximum stability. This is also caused by the multi-layer injection, which places more NO_x into lower layers (including the surface) and concentrations tend to build up as the lower atmosphere stabilizes and stratifies. Note that the largest differences tend to occur through the Ohio Valley and upper Midwest where the largest NO_x point sources exist. Other impacted areas include Tampa, Florida, the Gulf Coast, and central Texas.

Vertical NO_x concentration profiles are displayed in Figure 4-10 for the same hours as shown in Figures 4-6 and 4-8. The columns chosen for the NO_x profiles coincide with the surface grid cells containing the minimum and maximum NO_x differences. Concentration profiles for both the original and updated plume rise algorithm are compared. Figure 4-11 presents corresponding ozone profiles at the same hours and for the same grid columns. It is important to note that the concentration profiles are a result of potentially many different point sources injecting into these grid columns.

The largest positive surface NO_x difference during the June episode occurred on June 10, at 6 AM CST in a grid cell near Tampa, Florida. The surface concentration difference was less than 2 ppb, and this small variation extended upward through about 200m, where the peak concentration occurred. Above that level the updated plume rise resulted in a larger vertical gradient in NO_x up to about 400 m. This grid cell contained 68 individual point sources, with plume heights ranging from 45 to 300+ m. None of these plume heights were impacted by the updated plume rise algorithm. Instead, the updated plume rise resulted in a slightly larger quantity of NO_x in the shallow boundary layer, and lower NO_x in the capping stable layer, due to larger vertical spread of emission injection.

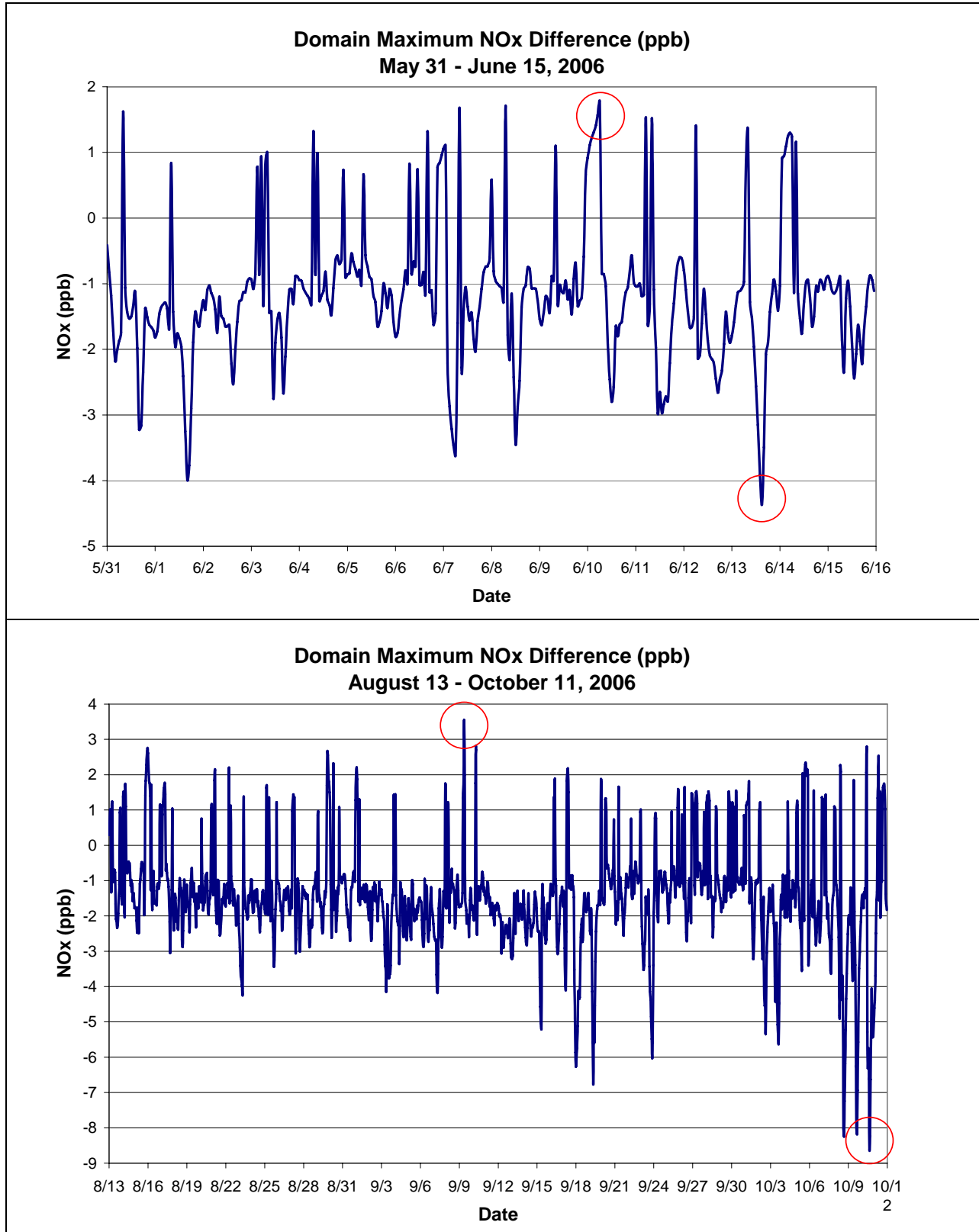


Figure 4-5. Hourly domain-wide peak NOx differences between two CAMx simulations of the TCEQ 2006 Houston modeling periods using the updated and original CAMx plume rise algorithm. Red circles highlight the hours shown in Figures 4-6 through 4-9.

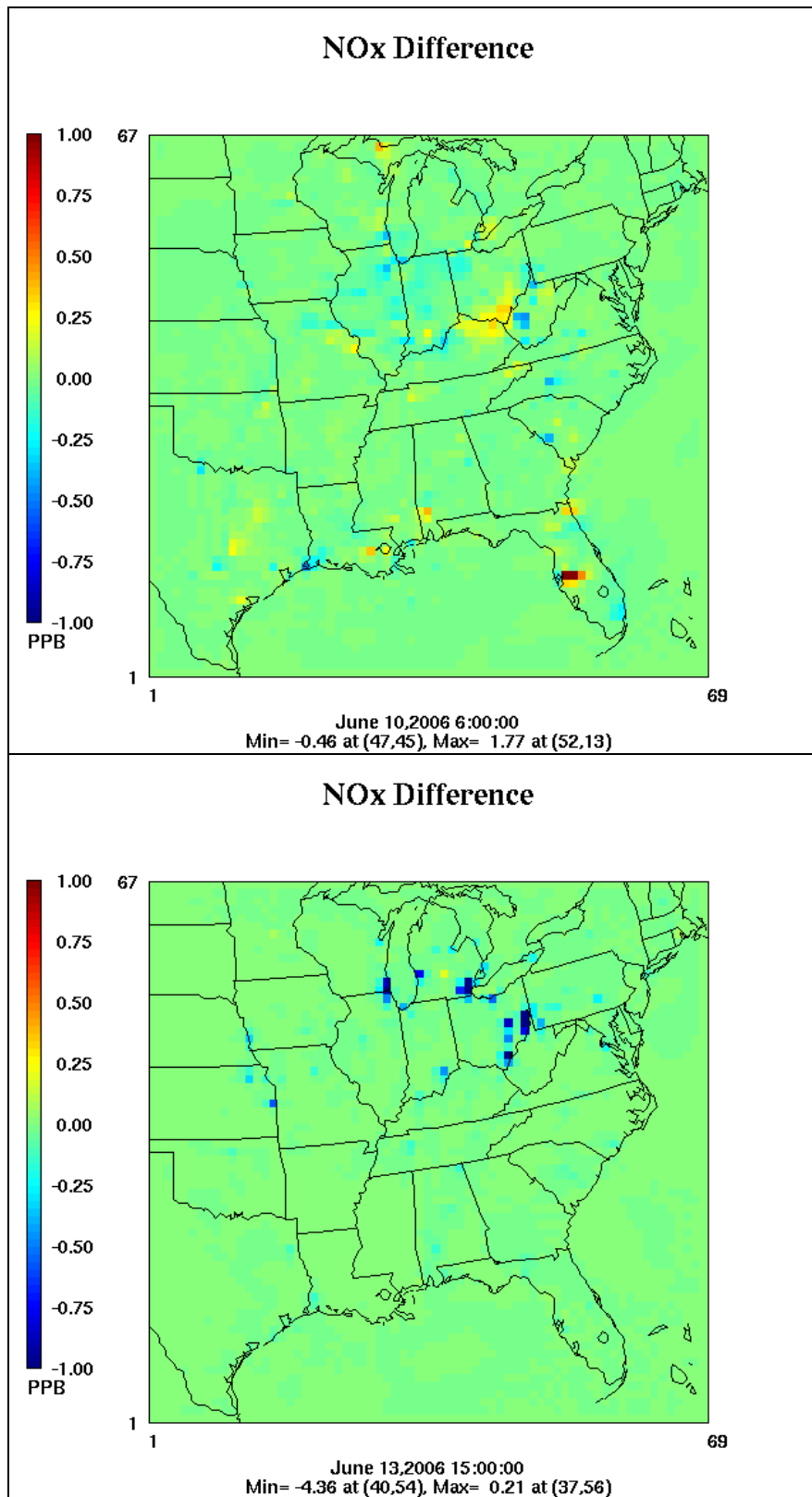


Figure 4-6. Domain-wide NOx differences during the hour of peak positive difference (top) and peak negative difference (bottom) during the June 2006 CAMx simulation using the updated and original CAMx plume rise algorithm.

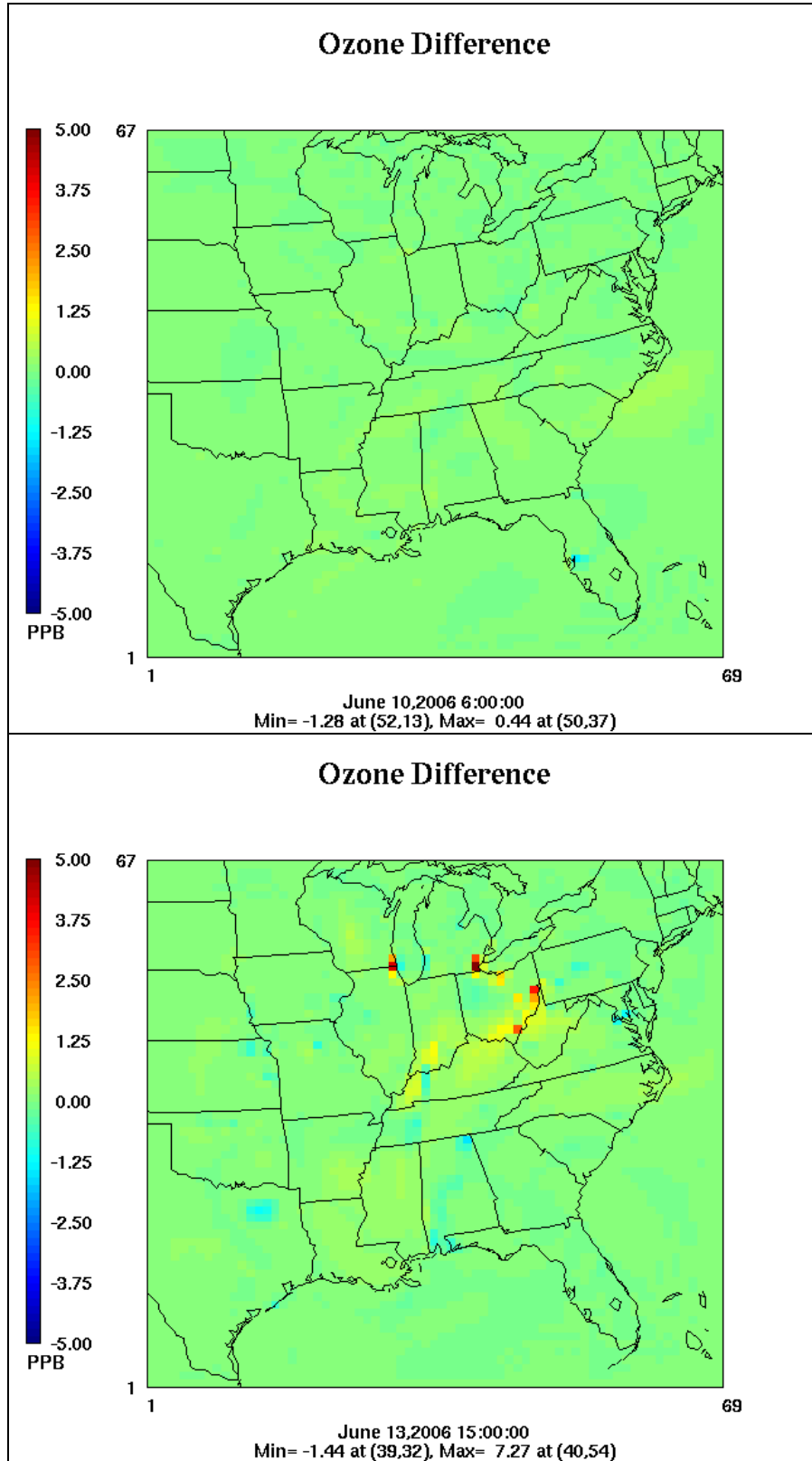


Figure 4-7. Domain-wide ozone differences for the same hours shown in Figure 4-6 during the June 2006 CAMx simulation using the updated and original CAMx plume rise algorithm.

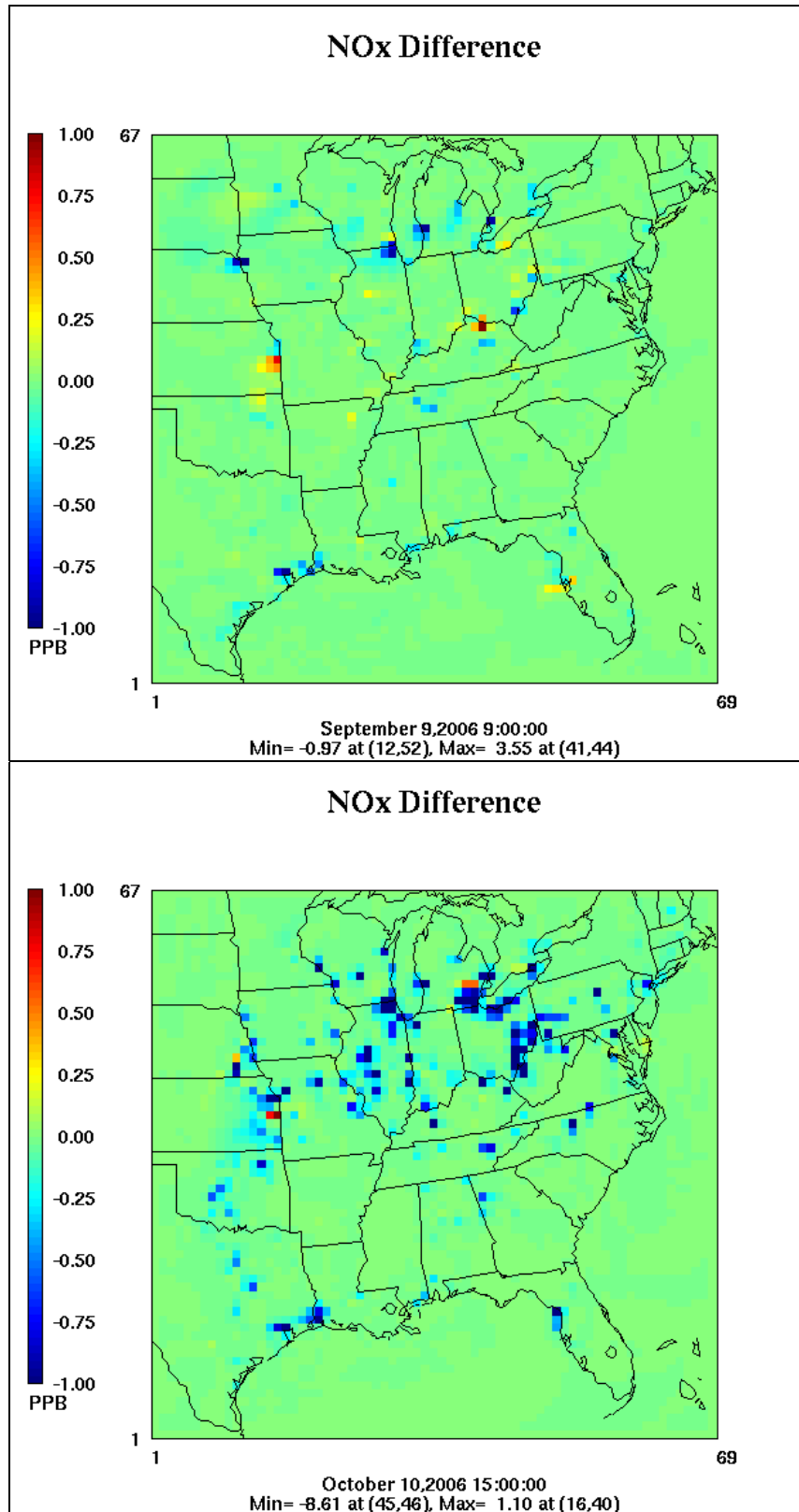


Figure 4-8. Domain-wide NOx differences during the hour of peak positive difference (top) and peak negative difference (bottom) during the August-October 2006 CAMx simulation using the updated and original CAMx plume rise algorithm.

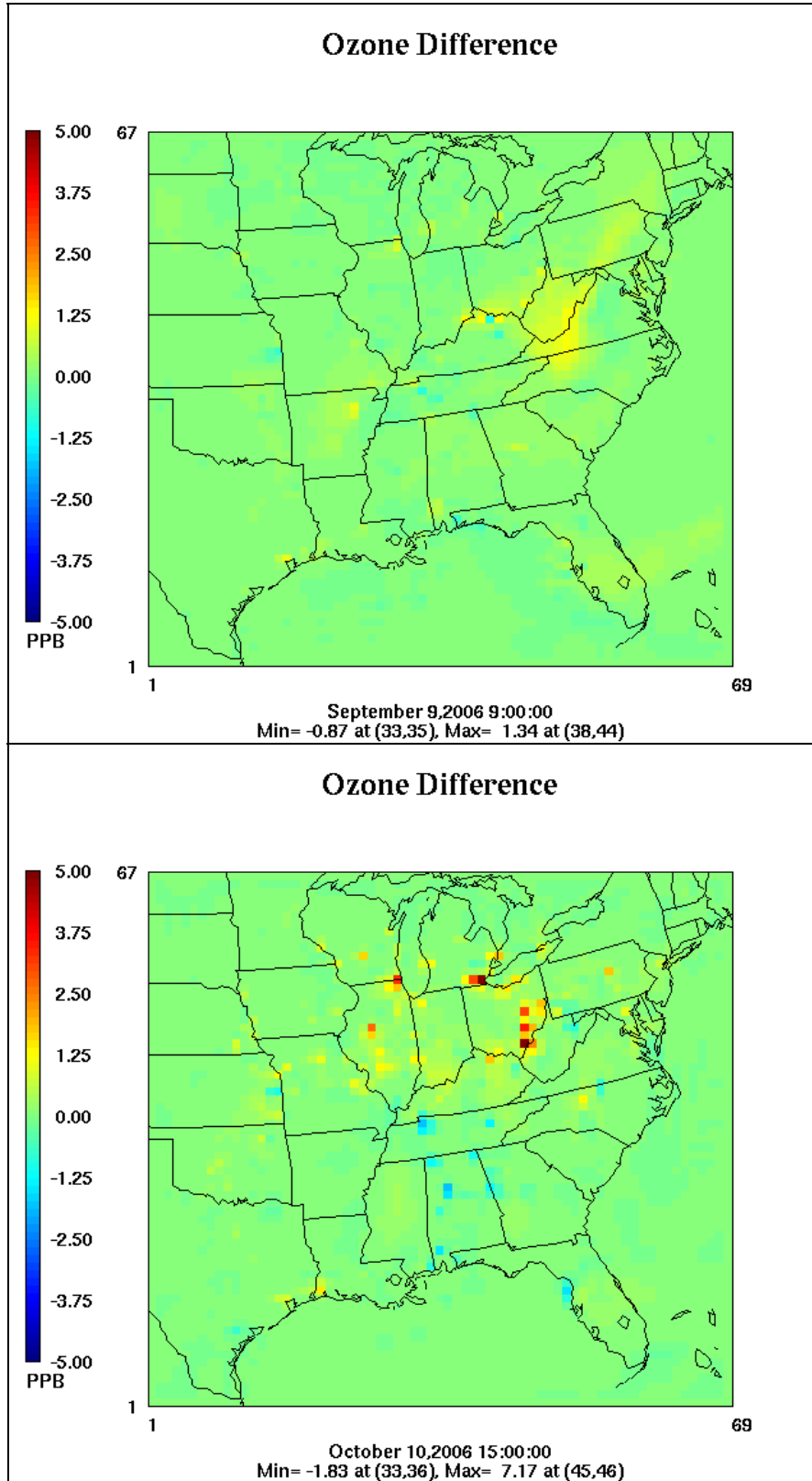


Figure 4-9. Domain-wide ozone differences for the same hours shown in Figure 4-8 during the August-October 2006 CAMx simulation using the updated and original CAMx plume rise algorithm.

On June 13 at 3 PM CST, the largest negative surface NO_x difference reached nearly -5 ppb in a grid cell near Detroit, Michigan. The well-mixed boundary layer is evident, as both NO_x profiles were nearly constant in height up to 800 m. The original plume rise algorithm resulted in a peak NO_x concentration of 10 ppb at about 860 m, while the updated plume rise algorithm put the peak NO_x at 1200 m. In this case, it is fairly obvious that the updated plume rise was much higher, and that portions of the NO_x plume were placed in upper stable layers. This reduced the total column NO_x put within the well mixed boundary layer. This grid cell contained 19 individual point sources, with plume heights ranging from 40 m to 1300+ m in the updated case. Plume rise for only two of the highest reaching point sources were impacted by the updated algorithm, resulting in an additional 370 m rise (about 40%). Plume depths for these two sources ranged from 200 to 600 m.

The largest positive surface NO_x difference in the August-October episode occurred on September 9 at 9 AM CST in a grid cell near Cincinnati, Ohio. The surface NO_x difference was 3.5 ppb, and expanded with height to a maximum of about 8 ppb, where an elevated NO_x layer occurred at about 700 m in the updated plume rise case. The original plume rise algorithm placed a NO_x layer much higher, peaking around 1200 m. This grid cell contained 13 individual point sources, with plume heights ranging from 90 m to 620 m in the updated case. Two sources experienced plume height increases of +70 to +80 m, while the four highest sources had plume height decreases of -50 to -70 m and spread their plumes through 200 m of depth. The only modification that would lead to reduced plume rise is the application of minimum 1 m/s wind speed to control unrealistically high rise during quiescent conditions. However, these relatively small changes in plume heights do not explain how a peak NO_x concentration existed at 1200 m in the original case. We can only assume that it was derived from point source emissions in upstream cells that were significantly impacted by the updated plume rise algorithm. Given the time of day, the original NO_x peak at 1200 m seems too high, while the updated NO_x peak at 700 m appears more reasonable. Since the updated plume rise placed more mass through a lower and deeper set of layers, more NO_x was mixed into the growing boundary layer.

The largest negative surface NO_x difference occurred on October 10 at 3 PM CST in a grid cell on the Ohio/West Virginia border. The difference of -8 to -9 ppb was consistent through the entire boundary layer up to about 550 m. Similarly to the June 13 plot, the updated plume rise algorithm led to more mass injection into the capping stable layer, and less into the boundary layer. This grid cell contained 9 individual point sources, with plume heights ranging from 550 m to 840 m in the updated case. All but one source experienced higher plume rise of 160 m to 200 m (roughly 30%). Plume depths ranged from 100 to over 500 m.

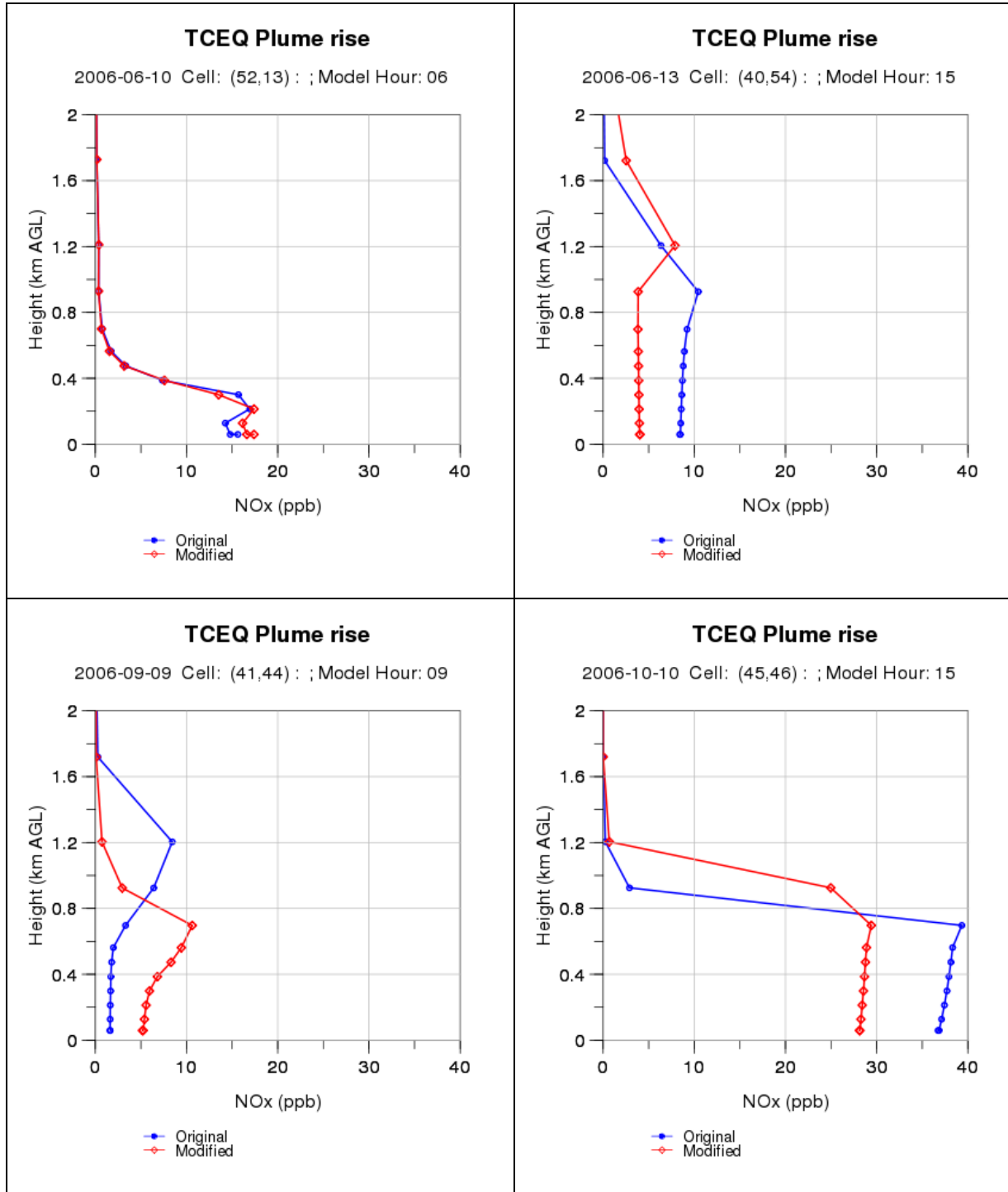


Figure 4-10. NOx concentration profiles at selected hours during the June 2006 (top) and August-October 2006 (bottom) CAMx simulations. Results are shown using the original plume rise algorithm (blue) and updated algorithm (red). Morning profiles on the left show episode-peak positive surface NOx concentrations. Afternoon profiles on the right show episode-peak negative surface NOx concentrations.

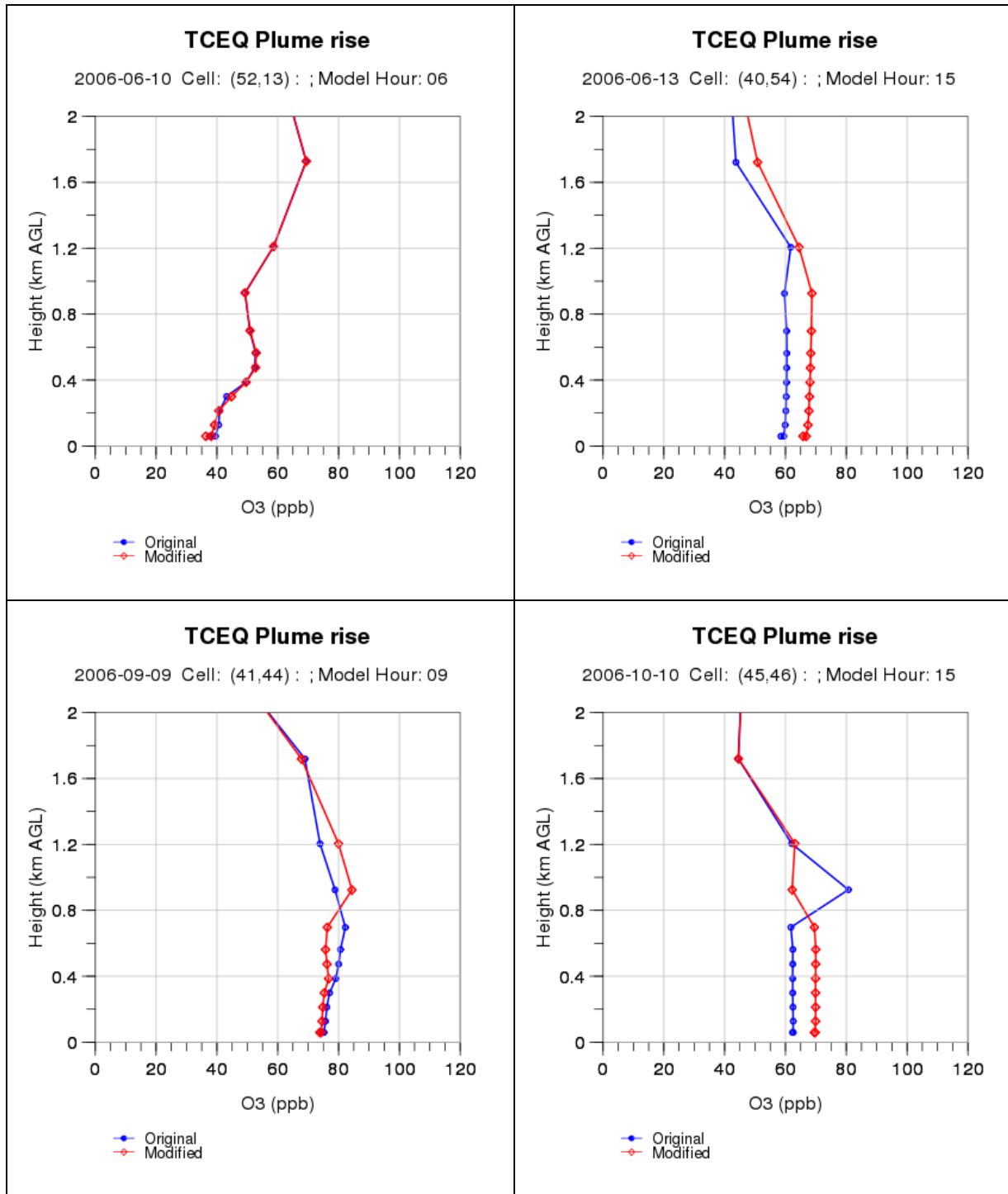


Figure 4-11. Ozone concentration profiles at selected hours during the June 2006 (top) and August-October 2006 (bottom) CAMx simulations. Results are shown using the original plume rise algorithm (blue) and updated algorithm (red). Dates and times are identical as Figure 4-10.

5. CONCLUSION

ENVIRON reviewed current plume rise algorithms used in several models (CAMx, SMOKE/CMAQ, CALPUFF, AERMOD) and initially recommended the SMOKE/CMAQ approach for consideration as an alternative option in CAMx. Comparing the CAMx and SMOKE/CMAQ plume rise calculations in a series of idealized tests revealed that, in most conditions tested, the CAMx and SMOKE/CMAQ plume rise estimates were very similar. However, some undesirable features were identified in the SMOKE/CMAQ plume rise calculations that led to counter-intuitive behavior across different wind speed and stability regimes, which included:

- The algorithm's complex logical branching structure leads to very discontinuous and often unexpected behavior as meteorological conditions cross internally defined thresholds;
- Related to the above, the algorithm results in lower plume rise under unstable/neutral conditions than stable conditions -- all other things being equal, plume rise should be higher under unstable than stable conditions (or at least the same);
- The algorithm is insensitive to stack or meteorological conditions for short stacks because it does not allow point source plume centerlines to exist in the first layer. This can result in a consistent upward bias for short stacks.
- The algorithm distributes mass to multiple model layers using a widely applied "rule-of-thumb" (Turner and Schulze, 2007) that assumes plume depth equals plume rise above the stack.
- An explicit mixing height is needed for the SMOKE/CMAQ algorithm, which may be difficult to specify in situations where the atmosphere has complex vertical structure, e.g., coastal environments.

Results of these tests were discussed with TCEQ and the SMOKE/CMAQ plume rise algorithm was dropped from consideration as an alternative to the CAMx plume rise algorithm. Instead, the remainder of the project focused on improving the current CAMx plume rise algorithm.

Based on the results presented in Section 3, we identified three specific modifications to the current CAMx plume rise algorithm:

1. Apply a lower limit to ambient wind speed (1 m/s minimum) to eliminate unrealistically large momentum and buoyancy rise under neutral/unstable light wind conditions;
2. Improve the layer-to-layer transition between neutral/unstable centerline rise to stable plume top rise that was leading to an artificial reduction in plume rise (particularly important for capping inversion cases);
3. Incorporate an algorithm to determine plume depth at final rise to allow for multi-layer plume injection, using diffusion equations developed for the plume-in-grid (PiG) sub-model rather than the "rule-of-thumb" approach of SMOKE/CMAQ.

Modifications (2) and (3) lead to improved plume emissions injection into the vertical layer structure plus partial plume penetration into a capping inversion.

The same idealized tests were run to evaluate the updated CAMx plume rise algorithm. In most cases, the original and updated plume rise estimates were identical. However, the updated plume rise

was improved for capping stable layer cases, and it resulted in deeper mass injection for stacks with slow exit velocities from which plumes take longer to reach final rise than plumes from fast stacks. In some capping inversions cases the plumes extended or “penetrated” into the capping inversion.

The updated plume rise algorithm was incorporated into CAMx version 5.20, and the model was run for two 2006 TCEQ Houston modeling periods over a single 36-km eastern U.S. domain. CAMx was run using the original and updated plume rise routines so that the impacts could be assessed over as many meteorological and geographical conditions as possible. Resulting CAMx surface concentration difference fields (new vs. original plume rise) for NO_x were screened over the entire modeling period, and specific grid columns were identified that contained the largest surface concentration impacts. Vertical NO_x and ozone concentration profiles for the selected grid columns were then compared for the standard and updated plume rise cases to evaluate changes in plume rise and depth.

Overall, surface NO_x differences tended to be small and negative, with peak differences remaining well within ± 10 ppb. Peak differences were weighted toward NO_x decreases, indicating that the plume rise update tends to lead toward either higher rise or more dilution by spreading emissions over multiple layers. In general, the plume rise update resulted in mostly NO_x reductions during daytime hours, while NO_x increases generally occurred during evening through early morning hours, periods of maximum stability. The largest impacts tended to occur through the Ohio Valley and upper Midwest in the autumn months.

Analysis of NO_x concentration profiles in the grid columns with the largest peak positive and negative surface NO_x concentration differences showed that the biggest impact of the plume rise updates were associated with injecting emissions over several layers. However, several cases of increased and reduced plume rise were noted. The multi-layer injection, coupled to occasional variations in plume rise (usually upwards), modulated the amount of NO_x in the boundary layer. This also impacted profiles of boundary layer ozone by altering the location and depth where ozone titration by fresh NO_x occurred.

This study has summarized the similarities and differences among the plume rise algorithms employed in the most widely used air quality models in the U.S. While our analyses show that these differences do not lead to significant impacts for modeling secondary pollutants such as ozone and PM, the same may not be true for applications that focus on concentrations of primary emissions near sources (e.g., toxics) and associated human exposure.

RECOMMENDATIONS

Based on the review and modeling analyses conducted in this study, we provide the following recommendations:

- The updated CAMx plume rise algorithm is an improvement and should be formally implemented as a replacement (not an option) for the current algorithm.
- The TCEQ should conduct additional tests comparing the original and updated plume rise schemes on their existing CAMx modeling datasets,
- An improved CMAQ plume rise algorithm should be developed and tested according to the updates incorporated in this study for CAMx.

6. REFERENCES

- Briggs, G.A. 1969. "Plume Rise: USAEC Critical Review Series." National Technical Information Service, Springfield, VA. 81pp (TID-25075).
- Briggs, G.A. 1971. Some Recent Analyses of Plume Rise Observation. In *Proceeding of the Second International Clean Air Congress*. H.M.Englund and W.T.Beery (eds.), Academic Press, New York. pp.1029-1032.
- Briggs, G.A. 1972. Discussion on chimney plumes in neutral and stable surroundings. *Atmos. Environ.*, **6**, 507-510.
- Briggs, G.A. 1975. Plume rise predictions. In *Lectures on Air Pollution and Environmental Impact Analyses*, Workshop Proceedings, Boston, MA, September 29 – October 3, 59-111.
- Briggs, G.A. 1984. Plume rise and buoyancy effects. In *Atmospheric Science and Power Production*, D. Randerson, Ed., Technical Information Center, U.S. Department of Energy, Oak Ridge, TN, 850 pp (DOE/TIC-27601).
- Byun, D.W., and F.S. Binkowski. 1991. "Sensitivity of RADM to Point Source Emissions Processing." Presented at the 7th Joint Conference on Applications of Air Pollution Meteorology of the American Meteorological Society and the Air and Waste Management Association, New Orleans, LA, January 14-18, 1991.
- Byun, D.W. and K. L. Schere. 2006. Review of the Governing Equations, Computational Algorithms, and Other Components of the Models-3 Community Multiscale Air Quality (CMAQ) Modeling System. *Applied Mechanics Reviews*, **59**, Number 2 (March 2006), pp. 51-77.
- ENVIRON. 2010. "User's Guide: Comprehensive Air quality Model with extensions, Version 5.20." Prepared by ENVIRON International Corporation, Novato, CA (April, 2010). Available at www.camx.com.
- EPA. 2004. "AERMOD: Description of Model Formulation." Prepared by the U.S. Environmental Protection Agency, Office of Air Quality Planning and Standards, Research Triangle Park, NC (September 2004). Available at http://www.epa.gov/scram001/7thconf/aermod/aermod_implmtn_guide_19March2009.pdf.
- EPRI. 2000. SCICHEM Version 1.2: Technical Documentation. Prepared by the Electric Power Research Institute, Palo Alto, California. (Report #1000713, December 2000).
- Houyoux, M.R. 1998. "Technical Report: Plume Rise Algorithm Summary for the Sparse Matrix Operator Modeling System (SMOKE)." MCNC – North Carolina Supercomputing Center, ENV-98TR004-v1.0.
- Louis, J.F. 1979. A Parametric Model of Vertical Eddy Fluxes in the Atmosphere. *Bound. Lay. Meteor.* **17**, 187-202.

- Peckham, S.E. et al. 2009. "WRF/Chem Version 3.1 User's Guide." Available at http://ruc.noaa.gov/wrf/WG11/Users_guide.pdf.
- Scire, J.S., D.G. Strimaitis, and R.J. Yamartino. 2000. "User's Guide for the CALPUFF Dispersion Model (Version 5)." Prepared by Earth Tech, Inc., Concord, MA (January, 2000). Available at http://www.dipic.unipd.it/Impianti/Profs/canu/files/ICA/EsercitazioneCALPUFF/CALPUFF_UsersGuide.pdf
- Seinfeld, J.H., and S.N. Pandis. 1998. *Atmospheric Chemistry and Physics, From Air Pollution to Climate Change*. John Wiley and Sons, Inc., NY.
- Turner, D.B. 1985. Proposed Pragmatic Methods for Estimating Plume Rise and Plume Penetration Through Atmospheric Layers." *Atmos. Env.*, **19**, 1215-1218.
- Turner, D.B., T. Chico, and A. Catalano. 1986. "TUPOS: A Multiple Source Gaussian Dispersion Algorithm Using On-Site Turbulence Data." U.S. Environmental Protection Agency, Research Triangle Park, North Carolina (EPA-600/8-86/010).
- Turner, D.B. and R.H. Schulze. 2007. *Practical Guide to Atmospheric Dispersion Modeling*. Air and Waste Management Association.
- UNC. 2009. "SMOKE V2.6 User's Manual." Available on-line at <http://www.smoke-model.org/version2.6/html/>.
- Weil, J.C. 1988. Plume rise. In *Lectures in Air Pollution Modeling*. A. Venkatram and J.C. Wyngaard, Eds., American Meteorological Society, 119-162.
- Weil, J.C., L.A. Corio, and R.P. Brower. 1997. A PDF dispersion model for buoyant plumes in the convective boundary layer. *J. Appl. Meteor.*, **36**, 982-1003.